2014

A transversely isotropic visco-hyperelastic constitutive model for soft tissues

Kulkarni, S.G.; Gao, X.-L.; Horner, S.E.; Mortlock, R.F.; Zheng, J.Q.

Sage

S.G. Kulkarni, X.-L. Gao, S.E. Horner, R.F. Mortlock, J.Q. Zheng. "A transversely isotropiv visco-hyperelastic constitutive model for soft tissues," Mathematics and Mechanics of Solids, v.31, no.6, (2014), pp. 747-770.
http://hdl.handle.net/10945/56668

Article

MMS

Mathematics and Mechanics of Solids
2016, Vol. 21(6) 747–770

DOI: 10.1177/1081286514536921
mms.sagepub.com
SAGE

A transversely isotropic visco-hyperelastic constitutive model for soft tissues

S G Kulkarni
Dassault Systemes Simulia Corp, Providence, RI, USA

X-L Gao
Department of Mechanical Engineering, Southern Methodist University, Dallas, TX, USA

S E Horner
Program Executive Office-SOLDIER, U.S. Army, VA, USA

R F Mortlock
Program Executive Office-SOLDIER, U.S. Army, VA, USA

J Q Zheng
Program Executive Office-SOLDIER, U.S. Army, VA, USA

Received 25 February 2014; accepted 1 May 2014

Abstract
A transversely isotropic visco-hyperelastic constitutive model is provided for soft tissues, which accounts for large deformations, high strain rates, and short-term memory effects. In the first part, a constitutive model for quasi-static deformations of soft tissues is presented, in which a soft tissue is simulated as a transversely isotropic hyperelastic material composed of a matrix and reinforcing fibers. The strain energy density function for the soft tissue is additively decomposed into two terms: a neo-Hookean function for the base matrix, and a polyconvex polynomial function of four invariants for the fibers. A comparison with existing experimental data for porcine brain tissues and bovine pericardium shows that this new model can well represent the quasi-static mechanical behavior of soft tissues. In the second part, a viscous potential is proposed to describe the rate-dependent short-term memory effects, resulting in a visco-hyperelastic constitutive model. This model is tested for a range of strain rates from 0.1 /s to 90 /s and for multiple loading scenarios based on available experimental data for porcine and human brain tissues. The model can be applied to other soft tissues by using different values of material and fitting parameters.

Keywords
Soft tissue, constitutive model, hyperelastic material, transversely isotropic material, strain energy, viscous potential, strain rate, elasticity tensor, viscosity tensor

Corresponding author:
X-L Gao, Department of Mechanical Engineering, Southern Methodist University, Dallas, TX 75275-0337, USA.
Email: xlgao@smu.edu

1. Introduction

Soft tissues represent body tissues that envelope, bind, connect, and support other body parts. Mechanical behavior of a soft tissue can be characterized by non-linear elastic deformations, strain rate sensitivity, hysteresis, viscoelastic responses (relaxation and creep), and permanent strains. Soft tissues have been extensively studied using continuum mechanics and non-linear elasticity [1, 2].

Brain tissues [3–6], spinal cord tissues [7, 8], and ligaments [9] have been found to be transversely isotropic. Body tissues exhibiting orthotropic material symmetry include cardiac tissues [10, 11] and arteries [2]. The current study is focused on the constitutive modeling of transversely isotropic soft tissues, which can be treated as hyperelastic or visco-hyperelastic materials.

For a hyperelastic or Green elastic material, a strain energy density function can be used to determine all stress components. One approach is to use a polynomial strain energy density function to describe the material response [12, 13]. The material parameters involved in such a polynomial function are numerous and often do not have any physical meaning. These models tend to be numerically unstable at high strains and violate convexity conditions [14]. Another approach is to work with a strain energy density function that contains two terms — one for the matrix and the other for the reinforcing fibers [14, 15]. The matrix is often modeled as a neo-Hookean material, a compressible Blatz-Ko material, or a Mooney-Rivlin solid. The most commonly used reinforcing model is the "standard reinforcing model" [2, 16]. In this model, the strain energy density function for the isotropic matrix is augmented by a term for the reinforcing fibers, which is a function (usually exponential or power) of a fourth invariant of the right Cauchy-Green deformation tensor. It is assumed that the fibers have no influence on the mechanical behavior of a soft tissue in compression, for its along-fiber shear deformation, or when it is stretched perpendicular to the fiber orientation.

Constitutive modeling of soft tissues as hyperelastic materials can also be conducted by using separate strain energy density functions for the matrix, fibers, and fiber–matrix interaction zone [17–19]. This additive decomposition of the total strain energy into three separate terms is based on the experimental finding that intralamellar fiber–fiber and fiber–matrix interactions make a significant contribution to soft tissue stiffness. To describe the interaction energy, Criscione et al. [18] proposed five physically-based invariants. A phenomenological model was developed by Peng et al. [8] for human annulus fibrosus by providing a new strain energy density function to account for the fiber–matrix shearing interaction. Guo et al. [20] explained the shear interaction based on mechanics of composites, which was also verified numerically [21].

The effect of strain rate on soft tissues is important, particularly for blast-induced traumatic brain injuries. Experiments have demonstrated that brain tissues are sensitive to the time scale of loading. A brain tissue responds immediately to loading, is sensitive to load variations, and remembers the history of loading [22]. It has been experimentally observed that shear responses of human brain tissues are rate-dependent [23–25]. Changes in strain rate generate additional amounts of stress in the soft tissue. Tensile/compressive responses of brain tissues are also found to be rate-dependent [26, 27]. Brain tissue responses under tension/compression loading stiffen considerably as the rate of loading increases [28]. Unlike shear responses, tensile/compressive responses are explicitly more sensitive at higher strain rates [26, 27]. This is of particular importance in modeling traumatic brain injuries (TBI) induced by blast events, where the duration of impact is on the order of milliseconds [29]. Explicit modeling of strain rate responses will help characterize tissue properties near impact sites (particularly useful in modeling TBI) over the expected range of loading rate.

In the current work, a new strain energy density function is proposed for soft tissues by modeling a soft tissue as a transversely isotropic composite consisting of a matrix (base) material and reinforcing fibers. The matrix is regarded as isotropic and described by using the neo-Hookean strain energy density function. Another function is used to represent the contributions from both fiber stretching and fiber–matrix interaction.

The rest of this paper is organized in the following manner. In Section 2, elements of continuum mechanics essential for the formulation are presented. In Section 3, a new strain energy density function for describing quasi-static responses of soft tissues is proposed and examined, and its predictions are compared with those by a standard reinforcing model. Relevant issues on the polyconvexity of the newly proposed strain energy density function and the ellipticity of the elasticity tensor are also briefly addressed. In Section 4, a viscous potential is proposed for simulating rate-dependent responses of soft

tissues (treated as transversely isotropic visco-hyperelastic materials), which is tested by comparing with experimental data available for different soft tissues at various strain rates. The paper concludes in Section 5 with a summary.

2. Elements of continuum mechanics

2.1. Kinematics

Let $\mathbf{X}$ be the position vector of a material point in the undeformed (reference) configuration, and $\mathbf{x}$ be the corresponding position vector in the deformed configuration. The latter is related to the former through the equation of motion

$$\mathbf{x} = \chi(\mathbf{X}, t), \tag{1}$$

where χ is a function describing the motion. The deformation gradient tensor, $\mathbf{F}$, is given by

$$\mathbf{F} = \frac{\partial \mathbf{x}}{\partial \mathbf{X}}, \tag{2}$$

which is a two-point tensor mapping the vector $d\mathbf{X}$ in the reference configuration to the vector $d\mathbf{x}$ in the deformed configuration (i.e., $d\mathbf{x} = \mathbf{F}d\mathbf{X}$). It is required that $\mathbf{F}$ satisfy

$$J \equiv \det \mathbf{F} > 0, \tag{3}$$

where J is the Jacobian representing the ratio of the deformed volume dv to the undeformed volume dV (i.e., $dv = JdV$).

The right and left Cauchy-Green deformation tensors are, respectively, given by

$$\mathbf{C} = \mathbf{F}^T\mathbf{F}, \quad \mathbf{B} = \mathbf{F}\mathbf{F}^T, \tag{4a, b}$$

where the superscript T denotes the transpose of the tensor.

The three principal invariants of $\mathbf{C}$ are defined as

$$I_1 = tr\mathbf{C}, \quad I_2 = \frac{1}{2}\left[(tr\mathbf{C})^2 - tr(\mathbf{C}^2)\right], \quad I_3 = \det \mathbf{C}, \tag{5}$$

which are identical to those of $\mathbf{B}$. For an incompressible material, $I_3 = J^2 = 1$. For an isotropic hyperelastic material, the strain energy density function can be constructed using these three invariants, which form an integrity basis [30–32].

For a transversely isotropic hyperelastic material with a preferred (fiber) direction described by the unit vector $\mathbf{a}_0$ in the reference configuration, two additional invariants defined by

$$I_4 = \mathbf{a}_0 \cdot \mathbf{C}\mathbf{a}_0, \quad I_5 = \mathbf{a}_0 \cdot \mathbf{C}^2\mathbf{a}_0 \tag{6}$$

are needed in the invariant formulation of the constitutive equations [33]. If the reinforcing fibers are considered inextensible, then $I_4 = 1$.

It should be mentioned that the number of invariants (i.e., five) required in the invariant formulation corresponds to the number of independent stiffness or compliance constants needed for characterizing a transversely isotropic linearly elastic material [34, 35]. A general discussion on the link between the invariant formulation and the linearized elastic moduli of a transversely isotropic material has been provided by Schröder and Neff [36].

Note that among the five invariants defined in equations (5) and (6) only I_3 and I_4 can be physically interpreted, with $\sqrt{I_3}$ and $\sqrt{I_4}$ being, respectively, the volume ratio and the stretch in the fiber direction $\mathbf{a}_0$. This situation motivated the efforts in developing physically-based invariants, as alternatives to $I_1 \sim I_5$ defined in equations (5) and (6), for describing mechanical responses of transversely isotropic hyperelastic materials [18, 37, 38].

The rate of deformation tensor is given by

$$\mathbf{D} = \frac{1}{2}\left(\mathbf{L} + \mathbf{L}^T\right), \tag{7}$$

where $\mathbf{L} = \nabla \mathbf{v}$ is the velocity gradient. It can be readily shown that

$$\mathbf{L} = \dot{\mathbf{F}}\,\mathbf{F}^{-1}, \tag{8}$$

where the overhead dot represents the total time derivative, and the superscript "-1" denotes the inverse. It follows from equations 4(a), (7), and (8) that the total material time derivative of $\mathbf{C}$ is given by

$$\dot{\mathbf{C}} \equiv \frac{D\mathbf{C}}{Dt} = 2\mathbf{F}^T\mathbf{D}\mathbf{F}. \tag{9}$$

2.2. Stress tensors

For hyperelastic materials, the use of the principle of material frame indifference and the first and second laws of thermodynamics leads to

$$\mathbf{S} = 2\frac{\partial W}{\partial \mathbf{C}}, \tag{10}$$

where $\mathbf{S}$ is the second Piola–Kirchhoff (P-K) stress tensor, and $W\,(= W(\mathbf{C}))$ is the strain energy density function (measuring the strain energy per unit undeformed volume). The Cauchy stress (measuring the force per unit deformed area) can be computed from $\mathbf{S}$ in equation (10) as

$$\boldsymbol{\sigma} = 2J^{-1}\mathbf{F}\frac{\partial W}{\partial \mathbf{C}}\mathbf{F}^T. \tag{11}$$

Equations (10) and (11) are for compressible materials.

For incompressible materials with $J = 1$, equations (10) and (11) become

$$\mathbf{S} = 2\frac{\partial W}{\partial \mathbf{C}} - p\mathbf{C}^{-1}, \quad \boldsymbol{\sigma} = 2\mathbf{F}\frac{\partial W}{\partial \mathbf{C}}\mathbf{F}^T - p\mathbf{I}, \tag{12a, b}$$

where p is the hydrostatic pressure acting as a Lagrange multiplier (associated with the kinematic constraint $\det\mathbf{C} = 1$), and $\mathbf{I}$ is the second-order identity tensor.

For a transversely isotropic hyperelastic material, the strain energy density function can be constructed using the five invariants $I_1 \sim I_5$ [33], i.e.,

$$W = W(I_1, I_2, I_3, I_4, I_5), \tag{13}$$

where I_i (i$\in \{1, 2, 3, 4, 5\}$) are functions of $\mathbf{C}$ defined in equations (5) and (6). It then follows from equations 12(a) and (13), with the help of the chain rule, that

$$\mathbf{S} = 2\sum_{j=1}^{5}\frac{\partial W}{\partial I_j}\frac{\partial I_j}{\partial \mathbf{C}} - p\mathbf{C}^{-1}, \tag{14}$$

where

$$\frac{\partial I_1}{\partial \mathbf{C}} = \mathbf{I}, \quad \frac{\partial I_2}{\partial \mathbf{C}} = I_1\mathbf{I} - \mathbf{C}, \quad \frac{\partial I_3}{\partial \mathbf{C}} = I_3\mathbf{C}^{-1}, \quad \frac{\partial I_4}{\partial \mathbf{C}} = \mathbf{a}_0 \otimes \mathbf{a}_0, \quad \frac{\partial I_5}{\partial \mathbf{C}} = \mathbf{a}_0 \otimes \mathbf{C}\mathbf{a}_0 + \mathbf{C}\mathbf{a}_0 \otimes \mathbf{a}_0, \tag{15}$$

which are directly obtained from equations (5) and (6).

Using equation (15) in equation (14) gives the second P-K stress as

$$\mathbf{S} = 2\left[\left(\frac{\partial W}{\partial I_1} + I_1\frac{\partial W}{\partial I_2}\right)\mathbf{I} - \frac{\partial W}{\partial I_2}\mathbf{C} + \frac{\partial W}{\partial I_4}\mathbf{a}_0 \otimes \mathbf{a}_0 + \frac{\partial W}{\partial I_5}(\mathbf{a}_0 \otimes \mathbf{C}\mathbf{a}_0 + \mathbf{C}\mathbf{a}_0 \otimes a_0)\right] - p\mathbf{C}^{-1}, \tag{16}$$

where use has been made of $I_3 = 1$ for incompressible materials and the $\partial W/\partial I_3$ term has been consolidated with the hydrostatic pressure term.

Similarly, substituting equations (13) and (15) into equation (12b) results in, with the help of the Cayley-Hamilton theorem,

$$\boldsymbol{\sigma} = 2\left[\frac{\partial W}{\partial I_1}\mathbf{B} - \frac{\partial W}{\partial I_2}\mathbf{B}^{-1} + I_4\frac{\partial W}{\partial I_4}\mathbf{a} \otimes \mathbf{a} + I_4\frac{\partial W}{\partial I_5}(\mathbf{a} \otimes \mathbf{B}\mathbf{a} + \mathbf{B}\mathbf{a} \otimes \mathbf{a})\right] - p\mathbf{I} \tag{17}$$

as the Cauchy stress, where the $\partial W/\partial I_3$ term and one term containing $\partial W/\partial I_2$ have been consolidated with the hydrostatic pressure term. In equation (17), **a** is a unit vector along the fiber direction in the deformed configuration.

2.3. Constitutive laws

A constitutive law is required to describe the stress–strain relation of a material. A general constitutive law for a material of integral type is given by [39, 40]

$$\mathbf{S}(t) = \underbrace{\mathbf{S}_e(\mathbf{C}(t))}_{\substack{\text{Equilibrium}\\ \text{response}}} + \underbrace{\mathbf{S}_v(\dot{\mathbf{C}}(t); \mathbf{C}(t))}_{\substack{\text{Short-term}\\ \text{memory response}}} + \underbrace{\int_{\delta}^{\infty} \Sigma(\mathbf{G}(t-s), s; \mathbf{C}(t))ds}_{\substack{\text{Long-term}\\ \text{memory response}}}, \tag{18}$$

where $\mathbf{S}$ is the second P-K stress tensor, $\mathbf{S}_e$ is an equilibrium term representing the elastic response, $\mathbf{S}_v$ is the viscous stress tensor, Σ is a functional describing the history of $\mathbf{G}(t-s) = \mathbf{C}(t-s) - \mathbf{C}(t)$, t is the present time, and s is the elapsed time.

When only the short-term memory effect is included, equation (18) reduces to

$$\mathbf{S}(t) = \mathbf{S}_e(\mathbf{C}(t)) + \mathbf{S}_v(\dot{\mathbf{C}}(t); \mathbf{C}(t)), \tag{19}$$

where the first term is the elastic (equilibrium state) stress, and the second term is the rate-dependent viscous (non-equilibrium state) stress.

3. Quasi-static response

A quasi-static response represents an equilibrium response of a soft tissue as $t \to \infty$.

For transversely isotropic hyperelastic materials, it has been shown [33] that in addition to the three principal invariants I_1, I_2 and I_3 for isotropic materials, two invariants I_4 and I_5, which are defined in equation (6), are required to fully describe the material response. Note that the invariant I_4 is directly linked to the fiber stretch, and the invariant I_5 is related to the fiber stretch and registers the fiber–matrix shear interaction additionally.

The invariant I_4 has been extensively used to model soft tissues [2, 4, 14, 16, 41, 42]. As an example, a strain energy density function of the following decoupled form has been proposed:

$$W(I_1, I_2, I_4) = W_{matrix}(I_1, I_2) + W_{fiber}(I_4), \tag{20}$$

where $W_{fiber}(I_4)$ is a convex function of I_4 [14, 43]. Hyperelasticity models of the form shown in equation (20) are known as standard reinforcing models.

However, the invariant I_5 has rarely been used due to a lack of understanding of the energy contribution from the fiber–matrix interaction. By analogy with equation (20), a strain energy function involving I_5 can be defined to have the form:

$$W(I_1, I_2, I_5) = W_{matrix}(I_1, I_2) + W_{fiber}(I_5). \tag{21}$$

Merodio and Ogden [44–46] studied models involving the invariant I_5 and compared the resulting predictions with those by models containing the invariant I_4. They found that the constitutive models employing the strain energy density function of the form in equation (21) are considerably stiffer than those models based on the strain energy density function of the form in equation (20). They also showed that the models based on equation (21) can be numerically unstable, as I_5 can have multiple minima [46].

Schröder and Neff [36] proposed a variety of strain energy density functions for modeling transversely isotropic soft tissues based on the five invariants $I_1 \sim I_5$ defined in equations (5) and (6).

Balzani et al. [47] suggested a strain energy density function for biological soft tissues by using a mixed invariant K_3 defined by $K_3 = I_1 I_4 - I_5$. Physically, K_3 is a polynomial invariant that controls the deformation of an area element whose normal is lying in an isotropic plane of the transversely isotropic material and is perpendicular to $\mathbf{a}_0$ (the unit vector in the preferred fiber direction) [36]. This strain energy density function contains three or more material parameters and has been used to fit experimental data obtained under uniaxial tensile loading.

Motivated by the studies of Schröder and Neff [36] and Balzani et al. [47] and based on the observations that fibers have negligible compression stiffness (thereby not contributing to the strain energy when under contraction) and the fiber–matrix interaction affects the mechanical response of a soft tissue, the following strain energy density function is proposed for transversely isotropic soft tissues in the current study:

$$\begin{aligned} W_e &= \frac{\mu}{2}(I_1 - 3) + \mu_1 (K_4 - 7)^q, \\ K_4 &= I_2 + 2I_1 I_4 - 2I_5, \end{aligned} \tag{22}$$

where μ is the shear modulus for infinitesimal deformations, μ_1 is a material constant, q is an exponent (with $q > 1$), and K_4 is a mixed invariant introduced in Schröder and Neff [36]. As a polynomial function of the integrity bases $I_1 \sim I_5$, K_4 is invariant under the transverse isotropy material symmetry group, since $I_1 \sim I_5$ are all invariant under such transformations [47]. This newly proposed model has not been used before and will be examined here.

It is required that the strain energy density function and the second P-K stress be zero-valued in the reference configuration, where there is no deformation such that $\mathbf{F} = \mathbf{I}$, $\mathbf{C} = \mathbf{I}$, $I_1 = 3$, $I_2 = 3$, $I_3 = 1$, $I_4 = 1$, and $I_5 = 1$. Upon using equation (16), these requirements become

$$\begin{aligned} &W|_{I_1=3, I_2=3, I_3=1, I_4=1, I_5=1} = 0, \\ &(W_1 + 2W_2)|_{I_1=3, I_2=3, I_3=1, I_4=1, I_5=1} = \frac{p_0}{2}, \\ &(W_4 + 2W_5)|_{I_1=3, I_2=3, I_3=1, I_4=1, I_5=1} = 0, \end{aligned} \tag{23}$$

where $W_j \equiv \partial W / \partial I_j$ ($j = 1, 2, 3, 4, 5$), and p_0 is the value of the hydrostatic pressure in the reference configuration. It can be readily shown that equation (23) will be identically satisfied by W_e when p_0 is set to be μ. That is, the strain energy density function W_e proposed in equation (22) can satisfy the vanishing stress and energy conditions in the reference configuration.

Also, W_e can be shown to be polyconvex for $\mu > 0$, $\mu_1 > 0$, and $q > 1$, since I_1 and K_4 involved are polyconvex [36, 48]. The polyconvexity of this strain energy density function ensures the ellipticity of the corresponding acoustic tensor for all deformations [36, 49], thereby leading to numerically stable constitutive models.

To compare the new model proposed in equation (22) with standard reinforcing models of the form given in equation (20) in predicting transversely isotropic soft tissue responses, the following model is adopted:

$$W_e^S = \frac{\mu}{2}(I_1 - 3) - \frac{\mu_0}{2} J_m \ln\left[1 - \frac{(I_4 - 1)^n}{J_m}\right], \tag{24}$$

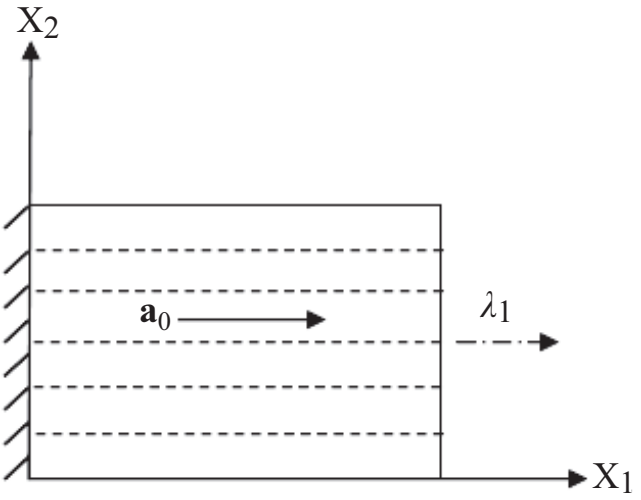

Figure 1. Uniaxial tension of a composite specimen with fibers and loading along the X_1 direction.

where μ_0 is a material constant, n is an exponent (with $n > 1$), and J_m is the limiting value of (I_1-3) accounting for the extensibility [16]. This model is a generalized version of one strain energy density function proposed by Horgan and Saccomandi [16] and is representative of the standard reinforcing models of the type shown in equation (20).

The feasibility of the new model proposed in equation (22) for describing constitutive behavior of transversely isotropic soft tissues will be studied along with that of the standard reinforcing model listed in equation (24) by fitting experimental curves obtained under different loading conditions in the remaining part of this section. The material is regarded as incompressible in the discussions herein.

3.1. Uniaxial loading

The stress responses to uniaxial loading along the X_1 direction predicted using W_e and W_e^S presented in equations (22) and (24) respectively are examined here. For this case, the reinforcing fibers are taken to be along the X_1 axis, as shown in Figure 1.

For uniaxial loading in the X_1 direction, the deformation gradient tensor $\mathbf{F}$ is given by

$$[F_{ij}] = \begin{bmatrix} \lambda_1 & 0 & 0 \\ 0 & \lambda_2 & 0 \\ 0 & 0 & \lambda_3 \end{bmatrix}, \tag{25}$$

where λ_1, λ_2 and λ_3, satisfying the incompressibility condition $\lambda_1\lambda_2\lambda_3 = 1$, are the principal stretches along the X_1, X_2 and X_3 directions, respectively.

The unit vector representing the fiber orientation in the reference and deformed configurations respectively reads

$$\mathbf{a}_0 = \mathbf{e}_1, \quad \mathbf{a} = \lambda_1 \mathbf{e}_1. \tag{26a, b}$$

For uniaxial loading along the fiber direction with $\lambda_2 = \lambda_3$, it follows from equations (4a), (5), (6), (22), (25) and (26a, b) that the invariants $I_1 \sim I_5$ and K_4 in this case are

$$I_1 = \lambda_1^2 + \frac{2}{\lambda_1}, \quad I_2 = 2\lambda_1 + \frac{1}{\lambda_1^2}, \quad I_3 = 1, \quad I_4 = \lambda_1^2, \quad I_5 = \lambda_1^4, \quad K_4 = 6\lambda_1 + \frac{1}{\lambda_1^2}. \tag{27}$$

For the strain energy density functions W_e and W_e^S presented in equations (22) and (24), equation (17) gives

$$\sigma_{11e} = 2\left[\frac{\mu}{2} + 2\mu_1 n I_4 (K_4 - 7)^{n-1}\right] B_{11} - 2\mu_1 n (K_4 - 7)^{n-1} B_{11}^{-1} + 4\mu_1 n I_1 (K_4 - 7)^{n-1} (\mathbf{a} \otimes \mathbf{a})_{11}$$
$$- 4\mu_1 n (K_4 - 7)^{n-1} (\mathbf{a} \otimes \mathbf{Ba} + \mathbf{Ba} \otimes \mathbf{a})_{11} - p,$$
$$\sigma_{11e}^S = \mu B_{11} + \frac{2\mu_0 (I_4 - 1)^{n-1}}{1 - \frac{(I_4-1)^n}{J_m}} (\mathbf{a} \otimes \mathbf{a})_{11} - p^S, \tag{28}$$

where "e" in the subscript represents the hyperelastic response, and "S" in the superscript denotes the standard reinforcing model given in equation (24).

The deformation characterized by equation (25) is homogeneous. Hence, the equilibrium equations in the absence of body forces will be satisfied if the hydrostatic pressure p is a constant.

For uniaxial loading along the X_1 direction, $\sigma_{33} = 0$. This result gives, from W_e in equation (22), W_e^S in equation (24), and equations (17) and (26b),

$$p = \left[\mu + 4\mu_1 n I_4 (K_4 - 7)^{n-1}\right] B_{33} - 2\mu_1 n (K_4 - 7)^{n-1} B_{33}^{-1},$$
$$p^S = \mu B_{33}. \tag{29}$$

Using equations (29), (25), (4b), and (26b) in equation (28) then yields

$$\frac{\sigma_{11e}}{\mu} = 2\left[\frac{1}{2} + \gamma n I_4 (K_4 - 7)^{n-1}\right](\lambda_1^2 - \lambda_3^2) - \gamma n (K_4 - 7)^{n-1}(\lambda_1^{-2} - \lambda_3^{-2})$$
$$+ 2\gamma n I_1 (K_4 - 7)^{n-1} \lambda_1^2 - 4\gamma n (K_4 - 7)^{n-1} \lambda_1^4,$$
$$\frac{\sigma_{11e}^S}{\mu} = \lambda_1^2 - \lambda_3^2 + \frac{\gamma_0 (I_4 - 1)^{n-1}}{1 - \frac{(I_4-1)^n}{J_m}} \lambda_1^2, \tag{30}$$

where

$$\gamma_0 = \frac{2\mu_0}{\mu}, \quad \gamma = \frac{2\mu_1}{\mu} \tag{31}$$

are two dimensionless parameters.

The normal stress in the X_1 direction, σ_{11e}, induced by the uniaxial tensile loading in the fiber direction (with $\lambda_2 = \lambda_3$) is plotted in Figures 2 and 3. The numerical values of σ_{11e} and σ_{11e}^S shown in Figures 2 and 3 are obtained from equations (30) and (27). For illustration purposes, in the calculations, q in W_e and n in W_e^S vary from 1.5 to 5. Also, J_m in W_e^S is selected to be 4.3. This value has been used by Destrade et al. [50] to study soft tissues and is based on fitting experimental data for porcine brainstems [5].

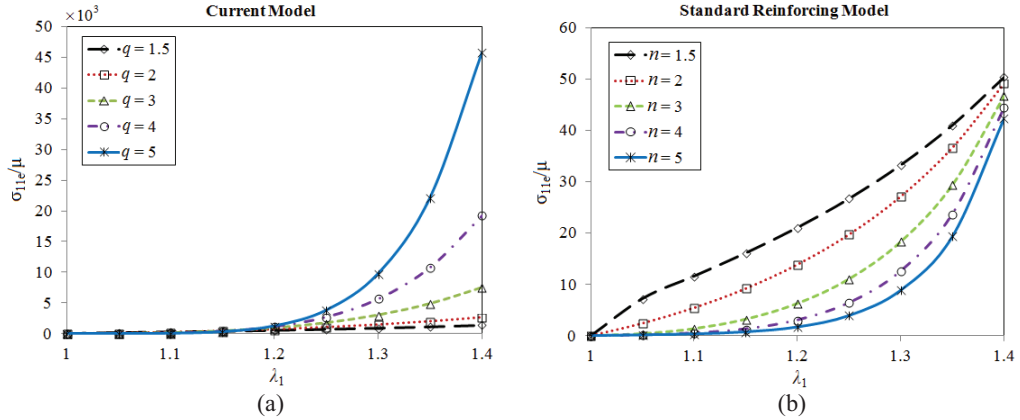

Figure 2. σ_{11e}/μ vs. λ_1 in the fiber direction: (a) current model with $\gamma = 10$; (b) standard reinforcing model with $J_m = 4.3$, $\gamma_0 = 10$.

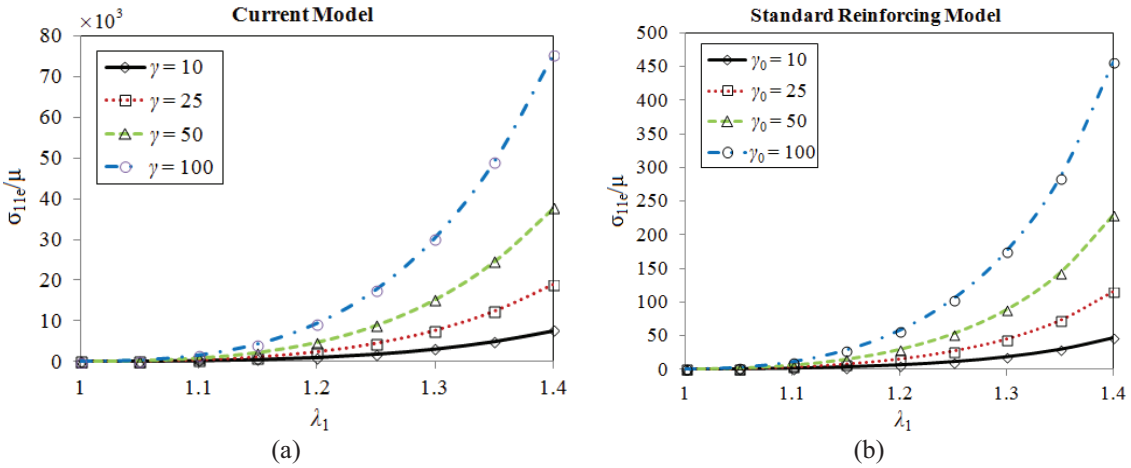

Figure 3. σ_{11e}/μ vs. λ_1 in the fiber direction: (a) current model with γ = 10, 25, 50, 100, q = 3; (b) standard reinforcing model with γ_0 = 10, 25, 50, 100, J_m = 4.3, n = 3.

Figures 2(a) and 2(b) illustrate the influence of the parameters q and n, respectively. Clearly, increasing the value of q in the current model based on equation (22) increases the stress contribution from the reinforcing fibers (see Figure 2(a)), while increasing the value of n in the standard reinforcing model based on equation (24) reduces the stress contribution from the reinforcing fibers (see Figure 2(b)). Also, it is seen that the effect of the parameter q is significant only when λ_1 is large. For small extensions, the curves with different values of q or n (for $n > 3$) are almost coincident. In particular, the stress response stiffens considerably at higher values of q.

Figures 3(a) and 3(b) show the effect of the parameters γ and γ_0, respectively, on the stress response predicted by the two models. It is observed that the stress σ_{11e} is a monotonically increasing function of the stretch for any value of γ or γ_0 considered.

3.2. Biaxial loading

For a planar biaxial deformation, the deformation gradient tensor $\mathbf{F}$ is given by

$$[F_{ij}] = \begin{bmatrix} F_{11} & F_{12} & 0 \\ F_{21} & F_{22} & 0 \\ 0 & 0 & F_{33} \end{bmatrix}, \tag{32}$$

where

$$F_{33} = \frac{1}{F_{11}F_{22} - F_{12}F_{21}} = \lambda_3. \tag{33}$$

It then follows from equations (4a, b)–(6) and (32) that the fiber direction in the deformed configuration and the five invariants are

$$\begin{aligned} &\mathbf{a} = \mathbf{F}\mathbf{a}_0 = (F_{11}\cos\theta + F_{12}\sin\theta)\mathbf{e}_1 + (F_{21}\cos\theta + F_{22}\sin\theta)\mathbf{e}_2, \\ &I_1 = B_{11} + B_{22} + B_{33}, \quad I_2 = B_{11}B_{22} + B_{11}B_{33} + B_{22}B_{33} - B_{12}^2, \quad I_3 = 1, \\ &I_4 = a_1^2 + a_2^2, \quad I_5 = B_{11}a_1^2 + 2B_{12}a_1a_2 + B_{22}a_2^2, \end{aligned} \tag{34}$$

where θ is the angle between the reinforcing fibers and the X_1 axis in the reference configuration, thereby giving $\mathbf{a}_0 = cos\theta\mathbf{e}_1 + sin\theta\mathbf{e}_2$. Note that in reaching the first expression in equation (34) it has been assumed that the fibers are inextensible with $\lambda = 1$, where λ is the stretch of the fiber along its direction $\mathbf{a}_0$, so that $\lambda\mathbf{a}(\mathbf{x}, t) = \mathbf{F}(\mathbf{X}, t)\mathbf{a}_0(\mathbf{X})$ reduces to $\mathbf{a} = \mathbf{F}\mathbf{a}_0$ [51].

Upon using the plane stress approximation ($\sigma_{33} = 0$), the expression for the hydrostatic pressure p can be obtained from equation (17) as, with $I_4 = 1$ for inextensible fibers,

$$p = 2\frac{\partial W}{\partial I_1}B_{33} - 2\frac{\partial W}{\partial I_2}B_{33}^{-1} + 2\frac{\partial W}{\partial I_4}(\mathbf{a}\otimes\mathbf{a})_{33} + 2\frac{\partial W}{\partial I_5}(\mathbf{a}\otimes\mathbf{Ba}+\mathbf{Ba}\otimes\mathbf{a})_{33}. \tag{35}$$

Using equation (35) in equation (17) gives the non-zero components of the Cauchy stress $\boldsymbol{\sigma}$ as

$$\begin{aligned}
\sigma_{11e} &= 2\frac{\partial W}{\partial I_1}(B_{11}-B_{33}) + 2\frac{\partial W}{\partial I_2}\left(B_{33}^{-1}-B_{11}^{-1}\right) + 2\frac{\partial W}{\partial I_4}\left[(\mathbf{a}\otimes\mathbf{a})_{11}-(\mathbf{a}\otimes\mathbf{a})_{33}\right] \\
&\quad + 2\frac{\partial W}{\partial I_5}\left[(\mathbf{a}\otimes\mathbf{Ba}+\mathbf{Ba}\otimes\mathbf{a})_{11}-(\mathbf{a}\otimes\mathbf{Ba}+\mathbf{Ba}\otimes\mathbf{a})_{33}\right], \\
\sigma_{22e} &= 2\frac{\partial W}{\partial I_1}(B_{22}-B_{33}) + 2\frac{\partial W}{\partial I_2}\left(B_{33}^{-1}-B_{22}^{-1}\right) + 2\frac{\partial W}{\partial I_4}\left[(\mathbf{a}\otimes\mathbf{a})_{22}-(\mathbf{a}\otimes\mathbf{a})_{33}\right] \\
&\quad + 2\frac{\partial W}{\partial I_5}\left[(\mathbf{a}\otimes\mathbf{Ba}+\mathbf{Ba}\otimes\mathbf{a})_{22}-(\mathbf{a}\otimes\mathbf{Ba}+\mathbf{Ba}\otimes\mathbf{a})_{33}\right], \\
\sigma_{12e} &= 2\frac{\partial W}{\partial I_1}B_{12} - 2\frac{\partial W}{\partial I_2}B_{12}^{-1} + 2\frac{\partial W}{\partial I_4}(\mathbf{a}\otimes\mathbf{a})_{12} + 2\frac{\partial W}{\partial I_5}(\mathbf{a}\otimes\mathbf{Ba}+\mathbf{Ba}\otimes\mathbf{a})_{12},
\end{aligned} \tag{36a–c}$$

where

$$\begin{aligned}
\left[(\mathbf{a}\otimes\mathbf{a})_{ij}\right] &= \begin{bmatrix} a_1^2 & a_1a_2 & 0 \\ a_2a_1 & a_2^2 & 0 \\ 0 & 0 & 0 \end{bmatrix}, \\
\left[(\mathbf{a}\otimes\mathbf{Ba})_{ij}\right] &= \begin{bmatrix} a_1(B_{11}a_1+B_{12}a_2) & a_1(B_{12}a_1+B_{22}a_2) & 0 \\ a_2(B_{11}a_1+B_{12}a_2) & a_2(B_{12}a_1+B_{22}a_2) & 0 \\ 0 & 0 & 0 \end{bmatrix}, \\
\left[(\mathbf{Ba}\otimes\mathbf{a})_{ij}\right] &= \begin{bmatrix} a_1(B_{11}a_1+B_{12}a_2) & a_2(B_{11}a_1+B_{12}a_2) & 0 \\ a_1(B_{12}a_1+B_{22}a_2) & a_2(B_{12}a_1+B_{22}a_2) & 0 \\ 0 & 0 & 0 \end{bmatrix}.
\end{aligned} \tag{37}$$

If there is no shear deformation, then the deformation gradient tensor is a diagonal matrix of the form *diag* $[\lambda_1\ \lambda_2\ \lambda_3]$, with $\lambda_3 = 1/(\lambda_1\lambda_2)$ (due to incompressibility). For this special case, W is a function of only two independent stretches, λ_1 and λ_2, in addition to the fiber angle θ. However, if the symmetry axis of the transversely isotropic material is not aligned with one loading direction, then a shear stress is required to maintain a homogeneous deformation in the specimen. In such a case, the deformation gradient tensor will have the form given in equation (32).

Figures 4 and 5 show the tensile stress–stretch curves for σ_{11e} and σ_{22e} in a specimen with the fiber direction along the X_1 axis subjected to equi-biaxial extension (with zero shear deformation), which are obtained from equations (36a, b) with $\theta = 0$ (i.e., the fiber orientation in this case is along the X_1 axis).

It is seen from Figures 4(a) and 4(b) that the axial normal stress–stretch curves predicted by both the models for the biaxial loading case are similar to those predicted for the uniaxial loading case (see Figures 2(a) and 2(b)).

However, the normal stress responses in the direction transverse to the fiber direction (i.e., the X_1 axis) predicted by the current model are significantly different from those predicted by the standard reinforcing model, as shown in Figures 5(a) and 5(b). The current model predicts σ_{22e}–λ_2 curves exhibiting stiffening responses (similar to those exhibited by the σ_{11e}–λ_1 curves (see Figures 4(a) and 5(a)), which is typical of the strain-hardening behavior experimentally displayed by soft tissues [4]. On the other hand, the standard reinforcing model predicts an increasing extensibility with increasing stress, with no stiffening effect observed (see Figure 5(b)).

What is shown in Figure 5(b) can be explained as follows. For the fiber orientation along the X_1 axis, $\theta = 0$ and $F_{12} = F_{21} = 0$. It then follows from equations (32) and (34) that for the equi-biaxial deformation considered,

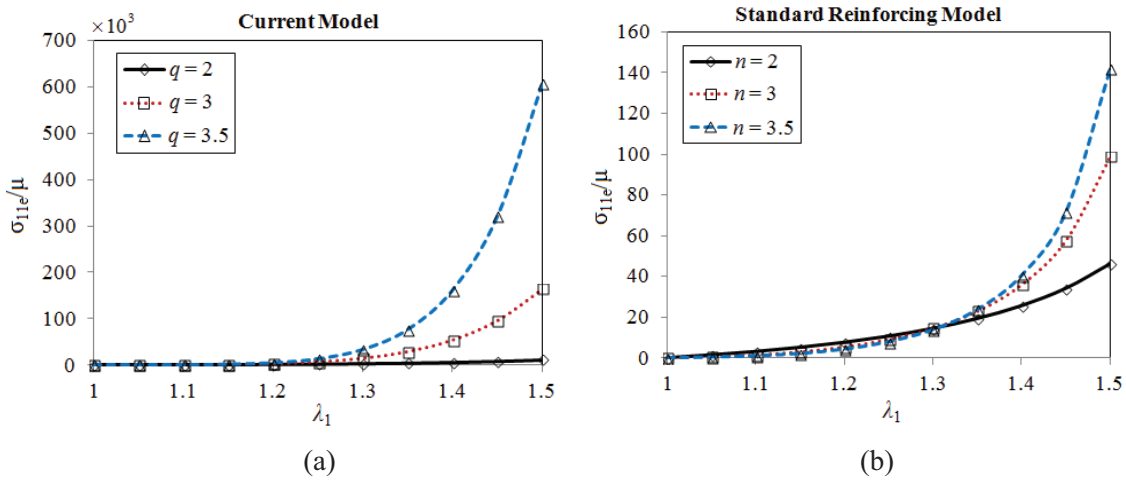

Figure 4. σ_{11e} vs. λ_1 in a specimen with the fiber direction along the X_1 axis subjected to equi-biaxial extension: (a) predictions by the current model with γ = 10; (b) predictions by the standard reinforcing model with J_m = 4.3, γ_0 = 10.

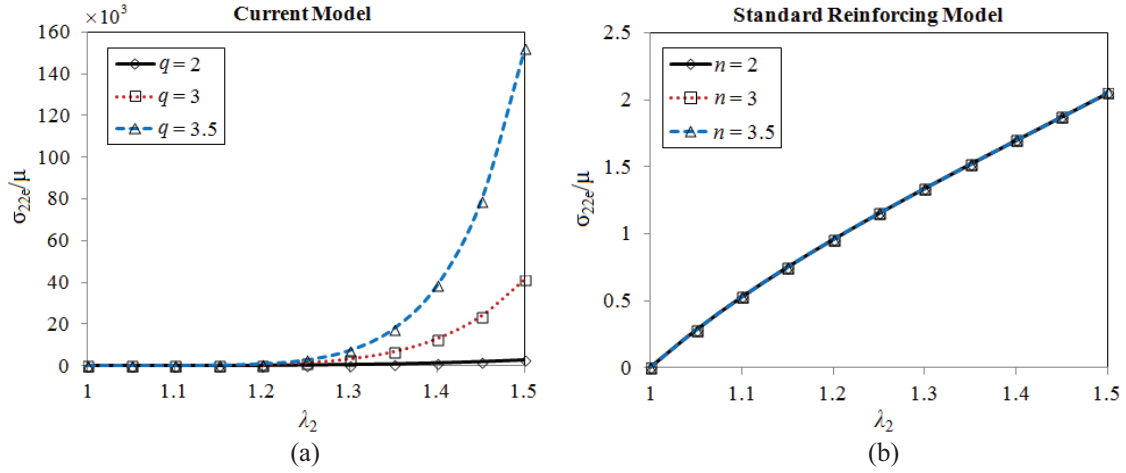

Figure 5. σ_{22e}/μ vs. λ_2 (=λ_1) in a specimen with the fiber direction along the X_1 axis subjected to equi-biaxial extension: (a) predictions by the current model with γ = 10; (b) predictions by the standard reinforcing model with J_m = 4.3, γ_0 = 10.

$$[F_{ij}] = \begin{bmatrix} \lambda_1 & 0 & 0 \\ 0 & \lambda_2 & 0 \\ 0 & 0 & \lambda_1^{-1}\lambda_2^{-1} \end{bmatrix}, \tag{38}$$

$$\mathbf{a} = \lambda_1 \mathbf{e}_1,$$

$$I_1 = \lambda_1^2 + \lambda_2^2 + \lambda_1^{-2}\lambda_2^{-2}, \quad I_2 = \lambda_1^2\lambda_2^2 + \lambda_2^{-2} + \lambda_1^{-2}, \quad I_3 = 1, \quad I_4 = \lambda_1^2, \quad I_5 = \lambda_1^4.$$

Using equation (38) and the expressions of W_e and W_e^S presented in equations (22) and (24) in equation (36b) yields

$$\sigma_{22e} = 2\left[\frac{\mu}{2} + 2\mu_1 q I_4 (K_4 - 7)^{q-1}\right](B_{22} - B_{33}) + 2\mu_1 q (K_4 - 7)^{q-1}\left(B_{33}^{-1} - B_{22}^{-1}\right),$$

$$\sigma_{22e}^S = \mu(B_{22} - B_{33}). \tag{39a, b}$$

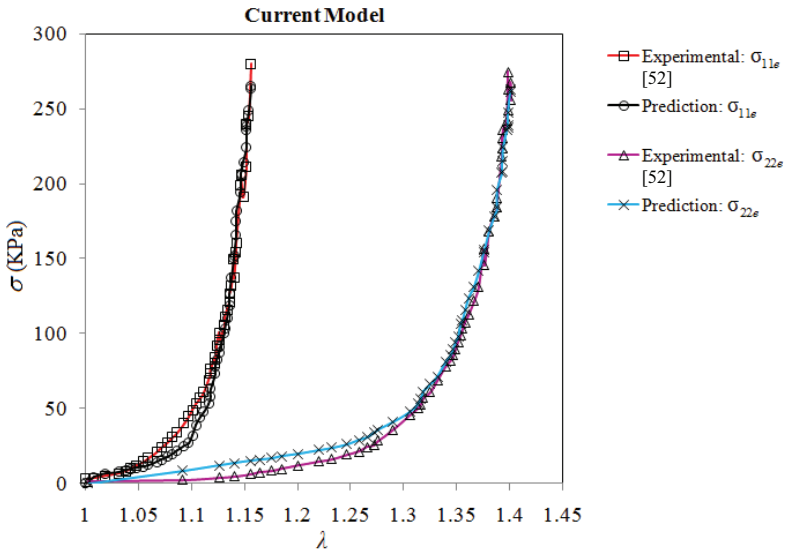

Figure 6. Comparison of the predictions by the current model with the equi-biaxial tension test data for bovine pericardium of Sacks [52]. The parameter values used are $q = 5.01$, $\gamma = 0.0018734$, $\mu = 23467.24$ Pa, and $\mu_1 = 21.94$ Pa.

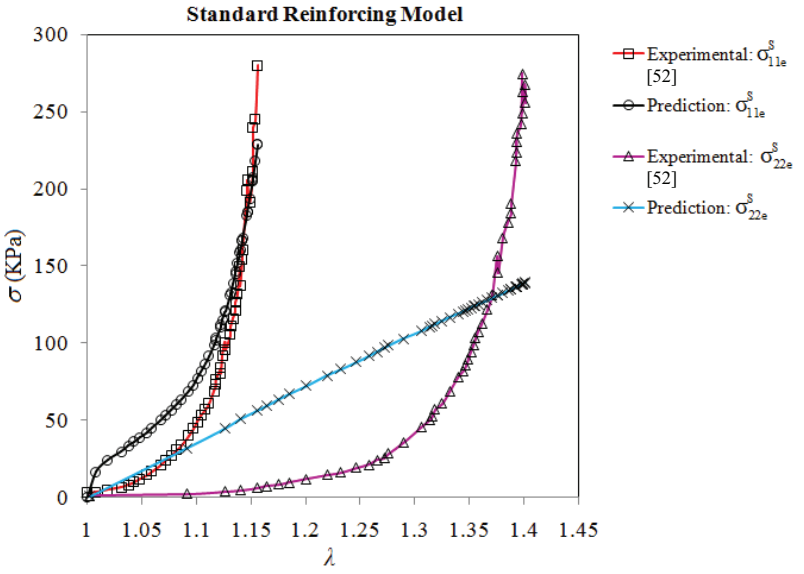

Figure 7. Comparison of the predictions by the standard reinforcing model with the equi-biaxial tension test data for bovine pericardium of Sacks [52]. The parameter values used are $n = 5.7$, $\gamma_0 = 224.235$, $\mu = 88123.53$ Pa, $\mu_0 = 9880211.14$ Pa, and $J_m = 4.3$.

It can be seen from equation (39b) that σ_{22e} predicted by the standard reinforcing model contains no contribution from the reinforcing fibers (represented by $W_{fiber}(I_4)$), unlike that predicted by the current model (see equation (39a). Therefore, the σ_{22e}–λ_2 curves in Figure 5(b) are essentially those of a neo-Hookean solid based on equation (39b) that is derived from the first (neo-Hookean) term of W_e^S given in equation (24).

Next, the predictions by the two models are tested by comparing with the experimental data obtained by Sacks [52] for equi-biaxial testing of transversely isotropic soft tissues of bovine pericardium. It has been shown [7, 53] that material parameters determined only from uniaxial tension tests may not correctly describe biaxial deformation responses. Hence, the experimental data of Sacks [52] from equi-biaxial tensile tests are simultaneously fitted to σ_{11e} and σ_{22e} predicted by the current model and the

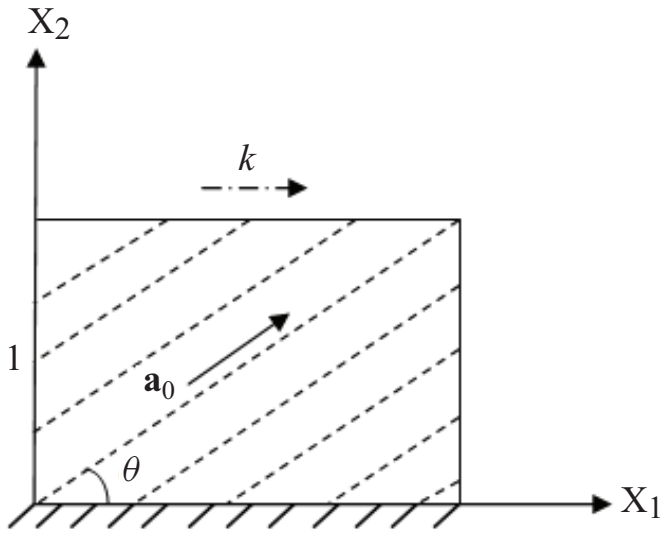

Figure 8. Simple shear deformation.

standard reinforcing model, respectively. The predicted and experimental σ_{11e}–λ_1 and σ_{22e}–λ_1 curves are shown in Figure 6 (for the current model) and Figure 7 (for the standard reinforcing model).

It is seen from Figure 6 that there is a fairly good agreement between the predictions by the current model and the experimental data. In contrast, the predictions by the standard reinforcing model do not agree very well with the experimental data, as shown in Figure 7. In addition, the transversely isotropic responses of the bovine pericardium soft tissues revealed by the experimental data are well captured by the current model, as shown in Figure 6.

For a general biaxial deformation with the deformation gradient tensor given in equation (32), the non-zero components of the Cauchy stress are σ_{11e}, σ_{22e}, σ_{33e}, σ_{12e}, and σ_{21e} ($= \sigma_{12e}$). Using a thin sheet approximation for soft tissues allows σ_{33e} to be set to zero, which then leads to the determination of the hydrostatic pressure p from equation (35). For the current model, the resulting three expressions for the non-zero stress components σ_{11e}, σ_{22e}, and σ_{12e} ($= \sigma_{21e}$) involve four independent constitutive functions, namely, $\partial W/\partial I_1$, $\partial W/\partial I_2$, $\partial W/\partial I_4$, and $\partial W/\partial I_5$, for the incompressible material (see equations (36a–c)). In order to fully characterize the transversely isotropic material properties, the minimum experimental tests required include: (a) planar biaxial tests with in-plane shear, and (b) through thickness shear tests. However, for membrane tissues (like brain tissues) where thin sections can be prepared, planar biaxial tests with an in-plane shear stress component would be sufficient for full characterization of the material properties. To the best of our knowledge, the current multi-axial experimental data available for transversely isotopic soft tissues are limited to equi-biaxial tests only.

3.3. Shearing deformation

Consider a simple shear deformation. When the simple shear of the amount k is applied in the X_1 direction, as shown in Figure 8, the deformation gradient tensor $\mathbf{F}$ is given by

$$[F_{ij}] = \begin{bmatrix} 1 & k & 0 \\ 0 & 1 & 0 \\ 0 & 0 & 1 \end{bmatrix}. \tag{40}$$

It follows from equations (4a), (5), (6) and (40) that

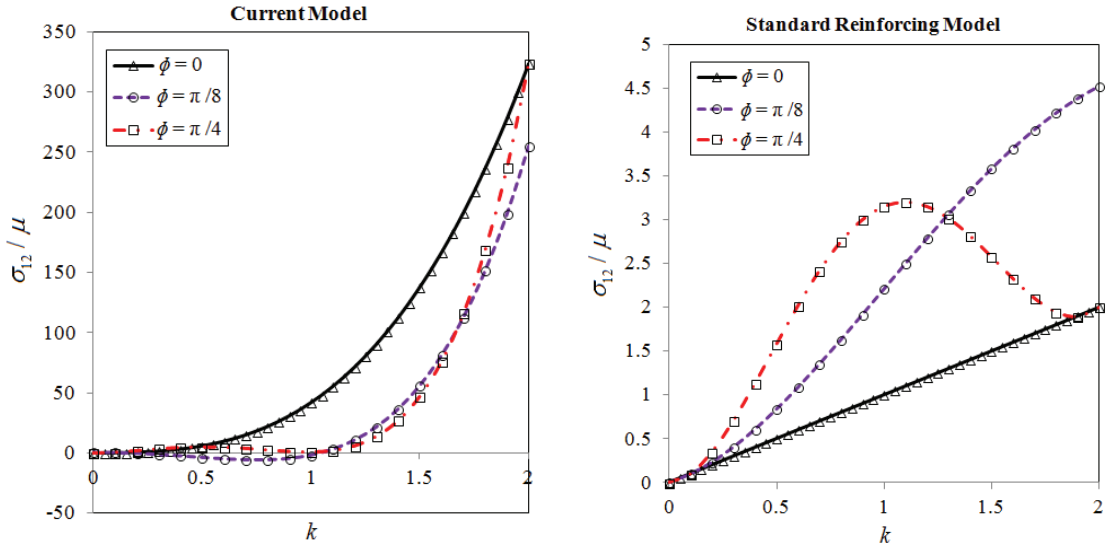

Figure 9. σ_{12}/μ vs. k for $\phi = 0$, $\pi/8$, $\pi/4$ and $\gamma_0 = \gamma = 20$, $n = 2$, $q = 2$, $J_m = 4.3$.

$$
\begin{aligned}
&I_1 = I_2 = 3 + k^2, \quad I_3 = 1,\\
&I_4 = 1 + k^2 \sin^2\theta + 2k \cos\theta \sin\theta,\\
&I_5 = 3k^2 \sin^2\theta + 4k \cos\theta \sin\theta + k^2(\cos\theta + k \sin\theta)^2 + 1.
\end{aligned}
\tag{41}
$$

Using equation (41) and the expressions of W_e and W_e^S presented in equations (22) and (24) in equation (17) then gives

$$
\begin{aligned}
\frac{\sigma_{12e}}{\mu} &= \left[1 + 2\gamma q I_4 (K_4 - 7)^{q-1}\right] k + \gamma q (K_4 - 7)^{q-1} k + 2\gamma q I_1 (K_4 - 7)^{q-1} \sin\theta(\cos\theta + k \sin\theta)\\
&\quad - 2\gamma q (K_4 - 7)^{q-1} \left\{(\cos\theta + k \sin\theta)\left[k(\cos\theta + k \sin\theta) + \left(2 + k^2\right) \sin\theta\right] + k \sin^2\theta\right\},\\
\frac{\sigma_{12e}^S}{\mu} &= k + \frac{\gamma_0 (I_4 - 1)^{n-1} \sin\theta(\cos\theta + k \sin\theta)}{1 - \frac{(I_4 - 1)^n}{J_m}}.
\end{aligned}
\tag{42}
$$

It follows from equation (41) that for the shear loading along the fiber direction (i.e., $\theta = 0$), $I_4 = 1$ and $K_4 = k^2 + 7$, and for the shear loading perpendicular to the fiber direction (i.e., $\theta = \pi/2$), $I_4 = k^2 + 1$ and $K_4 = 3k^2 + 7$. When $\theta = 0$, $I_4 = 1$ and the standard reinforcing model reduces to the neo-Hookean model, while the current model contains the second term depending on the shear strain k. For all other fiber directions (with $\theta \neq 0$ or $\pi/2$), K_4 can be obtained from equations (41) and (22) as $K_4 = 7 + k^2(1 + 2\sin^2\theta) + 2k \sin(2\theta)$.

For the simple shear loading in a direction ϕ relative to the X_1 axis in the X_1X_2 plane, the coordinate system with the following base vectors:

$$
\mathbf{e}_1 = \cos\phi \mathbf{i}_1 + \sin\phi \mathbf{i}_2, \quad \mathbf{e}_2 = -\sin\phi \mathbf{i}_1 + \cos\phi \mathbf{i}_2, \quad \mathbf{e}_3 = \mathbf{i}_3 \tag{43}
$$

is adopted such that the shear loading is along the $\mathbf{e}_1$ direction [54]. Note that the angle ϕ coincides with the angle θ only if the simple shear loading is along the fiber direction. In equation (43), $\mathbf{i}_1$, $\mathbf{i}_2$, and $\mathbf{i}_3$ are the base vectors associated with the coordinate system (X_1, X_2, X_3). The deformation gradient tensor is then given by

$$
\begin{aligned}
\mathbf{F} = \mathbf{I} + k\mathbf{e}_1 \otimes \mathbf{e}_2 &= (1 - k \sin\phi \cos\phi)\mathbf{i}_1 \otimes \mathbf{i}_1 + \left(k \cos^2\phi\right)\mathbf{i}_1 \otimes \mathbf{i}_2 - \left(k \sin^2\phi\right)\mathbf{i}_2 \otimes \mathbf{i}_1\\
&\quad + (1 + k \sin\phi \cos\phi)\mathbf{i}_2 \otimes \mathbf{i}_2 + \mathbf{i}_3 \otimes \mathbf{i}_3.
\end{aligned}
\tag{44}
$$

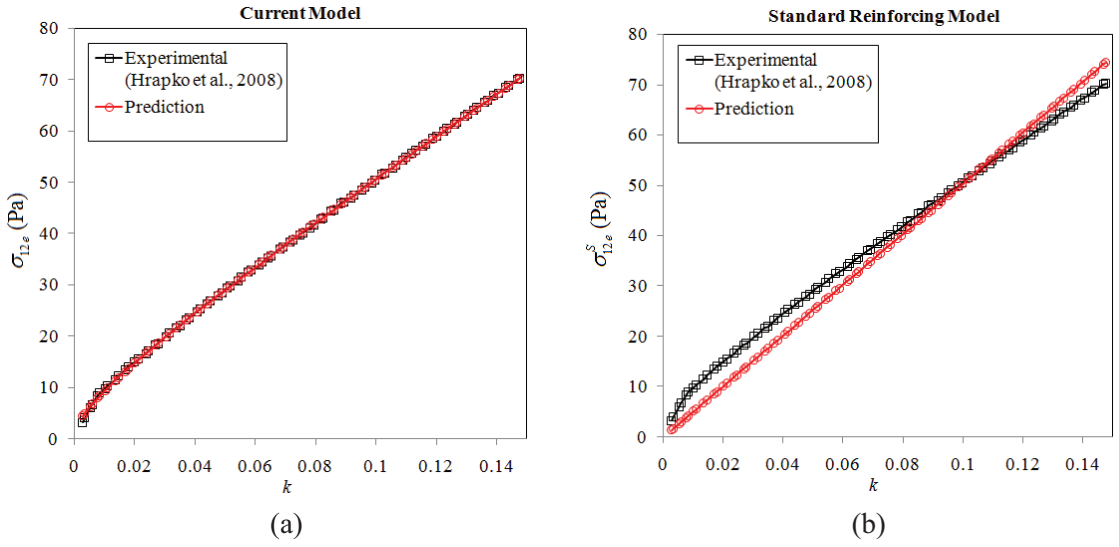

Figure 10. Comparison of the predictions with the experimental data of Hrapko et al. [24] for porcine brain tissues at the strain rate of 0.1 /s: (a) the current model with q = 0.7012, γ = 0.145, μ = 360.61 Pa, and μ_1 = 26.1804 Pa; (b) the standard reinforcing model with n =1, γ_0 = 0.07939, μ = 503.84 Pa, and μ_0 = 20 Pa.

It follows from equations (4a), (5), (6) and (44) that

$$\begin{aligned} I_1 &= 3 + k^2, \\ I_2 &= 3 + k^2, \\ I_4 &= 1 - k\sin(2\phi) + k^2\sin^2\phi, \\ I_5 &= 1 + k^2 + k\left(2 + k^2\right)\left[-\sin(2\phi) + k\sin^2\phi\right]. \end{aligned} \tag{45}$$

Also, for the fibers along the X_1 direction in the reference configuration (i.e., $\mathbf{a}_0 = \mathbf{i}_1$) and being inextensible

$$\mathbf{a} = \mathbf{F}\mathbf{a}_0 = (1 - k\sin\phi\cos\phi)\mathbf{i}_1 - k(\sin^2\phi)\,\mathbf{i}_2, \tag{46}$$

where use has been made of equation (44).

Figure 9 shows the variation of σ_{12}/μ with k predicted by both the models. From Figure 9, it is seen that for the case with $\phi = \pi/4$ the standard reinforcing model predicts unstable stress–strain behavior (i.e., decreasing shear stress for increasing shear strain) at high strains, while the current model predicts the stress–strain response that is commonly observed in soft tissues under shear loading [25, 55].

To test the efficacy of the newly proposed model in fitting experimental data, the predicted shear stress–strain curves are compared with the experimental curves provided in Hrapko et al. [24] for porcine brain tissues, as shown in Figure 10. Clearly, the predicted curves by the current model better capture the experimental curves for the brain tissues.

4. Rate-dependent response

Hyper-viscoelastic constitutive modeling combines the methodologies of viscoelasticity and hyperelasticity. One approach is to multiplicatively decompose the total deformation gradient tensor into an elastic part and a viscoelastic part [22] following the work of Lee [56]. The decomposition method of Lee [56] is based on the assumptions that the body is isotropic in the reference configuration and that the origin in the stress–temperature space always lies inside the loading surface [57]. As a result, this approach cannot be directly used to model anisotropic responses of soft tissues. Another approach to implementing

hyper-viscoelastic models is to decompose the deformation gradient tensor into a dilatational part and a volume-preserving part. This alternative approach is not restricted to any particular configuration.

For an isothermal deformation, the Clausius-Duhem inequality has the form [58–60]:

$$D_{int} = \frac{1}{2}\mathbf{S} : \dot{\mathbf{C}} - \dot{W}_e \geq 0, \tag{47}$$

where D_{int} is the internal dissipation, $\mathbf{S}$ is the second P-K stress, $\dot{\mathbf{C}}$ is the total material time derivative of $\mathbf{C}$ defined in equation (9), W_e is a hyperelastic strain energy density function, and $\dot{W}_e$ is the total time derivative of W_e. For $W_e = W_e(\mathbf{C})$, equation (47) can be rewritten as

$$D_{int} = \frac{1}{2}\left(\mathbf{S} - 2\frac{\partial W_e}{\partial \mathbf{C}}\right) : \dot{\mathbf{C}} \geq 0 \tag{48}$$

for any $\mathbf{C}$ and $\dot{\mathbf{C}}$.

For hyperelastic materials, the satisfaction of equation (48) for any $\dot{\mathbf{C}}$ requires that

$$\mathbf{S}_e = 2\frac{\partial W_e}{\partial \mathbf{C}}. \tag{49}$$

For materials with only the short-term memory effect, the second P-K stress $\mathbf{S}$ has the form given in equation (19). In order to account for the rate-dependent viscous effects observed in soft tissues, a viscous (or dissipative) potential of the following form can be introduced [39, 59]:

$$W_v = W_v(\dot{\mathbf{C}}; \mathbf{C}), \tag{50}$$

where $\dot{\mathbf{C}}$ is the variable and $\mathbf{C}$ is acting as a parameter. Since both $\mathbf{C}$ and $\dot{\mathbf{C}}$ are objective, equation (50) satisfies the material frame indifference principle. From equation (50), the internal dissipation D_{int} due to the viscous effects can be computed as

$$D_{int} = \frac{\partial W_v}{\partial \dot{\mathbf{C}}} : \dot{\mathbf{C}} \equiv \frac{1}{2}\mathbf{S}_v : \dot{\mathbf{C}} \tag{51}$$

for any $\mathbf{C}$ and $\dot{\mathbf{C}}$.

Combining equations (48), (49) and (51) yields

$$\mathbf{S} = \mathbf{S}_e + \mathbf{S}_v, \tag{52}$$

where $\mathbf{S}_e$, as the elastic part of the second P-K stress $\mathbf{S}$, is given in equation (49), and

$$\mathbf{S}_v = 2\frac{\partial W_v}{\partial \dot{\mathbf{C}}} \tag{53}$$

is the viscous part of $\mathbf{S}$.

For incompressible materials, equation (52) can be modified to obtain

$$\mathbf{S} = 2\frac{\partial W_e}{\partial \mathbf{C}} + 2\frac{\partial W_v}{\partial \dot{\mathbf{C}}} - p\mathbf{C}^{-1}, \tag{54}$$

where p is a hydrostatic pressure. Equation (54) provides a visco-hyperelastic constitutive law for incompressible materials with short-term memory effects.

In order to describe the short-term memory response of brain tissues, the following viscous potential is proposed in the current study:

$$W_v = \frac{1}{2}\mu_2 J_2 (I_1 - 3)^{n_1} + \mu_3 J_5 (K_4 - 7)^{n_2}, \tag{55}$$

Table 1. Values of the fitting parameters in W_e for quasi-static responses in tension and shear.

Parameters	Tensile response	Shear response
μ	279.41 Pa	359.74 Pa
μ_1	0.3315 Pa	0 Pa
q	6.7	1

Table 2. Values of the parameters in W_v for computing the viscous stress at different strain rates: uniaxial tension.

Strain rate (/s)	μ_2 (Pa·s^2)	μ_3 (Pa·s^2)	n_1	n_2	First-order optimality measure	Error	Data
0.1	4676.07	15.665	1	4.85	0.00121	0.0278	Prevost et al. [22]
1	4367.78	119.665	1	0.30	0.04273	0.0262	
4.3	0	95.29	1	0.823	0.1955	0.0597	Tamura et al. [27]
25	0	30.45	1	0.95	0.03202	0.04507	

Table 3. Values of the parameters in W_v for computing the viscous stress at different strain rates: along-fiber simple shear.

Strain rate (/s)	μ_2 (Pa·s^2)	μ_3 (Pa·s^2)	n_1	n_2	First-order optimality measure	Maximum Error	Data
0.1	19.971	170.79	1	0.19	2.667e-7	0.0201	Hrapko et al. [24]
1	302.72	50.7275	1	0.25	8.10e-6	0.0235	
15	0	209.46	1	0.52	0.00869	0.0472	Donnelly and Medige [25]
30	0	146.37	1	0.55	0.04608	0.0388	
60	0	57.585	1	0.43	0.54419	0.0581	
90	0	46.05	1	0.463	0.3086	0.04980	

where μ_2 and μ_3 are material constants, n_1 and n_2 are fitting exponents, and

$$J_2 = \frac{1}{2} tr\left(\dot{\mathbf{C}}^2\right), \quad J_5 = (\mathbf{a}_0 \otimes \mathbf{a}_0) : \dot{\mathbf{C}}^2 \tag{56}$$

are two invariants of $\dot{\mathbf{C}}$ [31, 59]. The general form of W_v that is invariant under the symmetry transformations of transverse isotropy is given in the appendix.

Using equation (55) in equation (53) gives

$$\mathbf{S}_v = \mu_2 (I_1 - 3)^{n_1} \dot{\mathbf{C}} + 2\mu_3 (K_4 - 7)^{n_2} \left[\mathbf{a}_0 \otimes \dot{\mathbf{C}}\mathbf{a}_0 + \dot{\mathbf{C}}\mathbf{a}_0 \otimes \mathbf{a}_0\right]. \tag{57}$$

It is clear from equation (57) that $\mathbf{S}_v = \mathbf{0}$ in the reference configuration where $\mathbf{F} = \mathbf{I}$ and $\dot{\mathbf{C}} = \mathbf{0}$ for any values of μ_2 and μ_3. Also, it follows from equation (57) that

$$\mathbf{S}_v : \dot{\mathbf{C}} = \mu_2 (I_1 - 3)^{n_1} \dot{\mathbf{C}} : \dot{\mathbf{C}} + 2\mu_3 (K_4 - 7)^{n_2} \left[\mathbf{a}_0 \otimes \dot{\mathbf{C}}\mathbf{a}_0 + \dot{\mathbf{C}}\mathbf{a}_0 \otimes \mathbf{a}_0\right] : \dot{\mathbf{C}} \geq 0 \tag{58}$$

for any $\mu_2 \geq 0$ and $\mu_3 \geq 0$. That is, the viscous potential proposed in equation (55) is thermodynamically admissible if $\mu_2 \geq 0$ and $\mu_3 \geq 0$.

To evaluate the newly proposed viscous potential presented in equation (55), predictions based on equation (57) (for $\mathbf{S}_v$) along with the quasi-static model proposed in equation (22) (for $\mathbf{S}_e$) are compared with the rate-dependent experimental data of Donnelly and Medige [25], Tamura et al. [27], and Prevost et al. [22]. The material constants for the new quasi-static model given in equation (22) are listed in

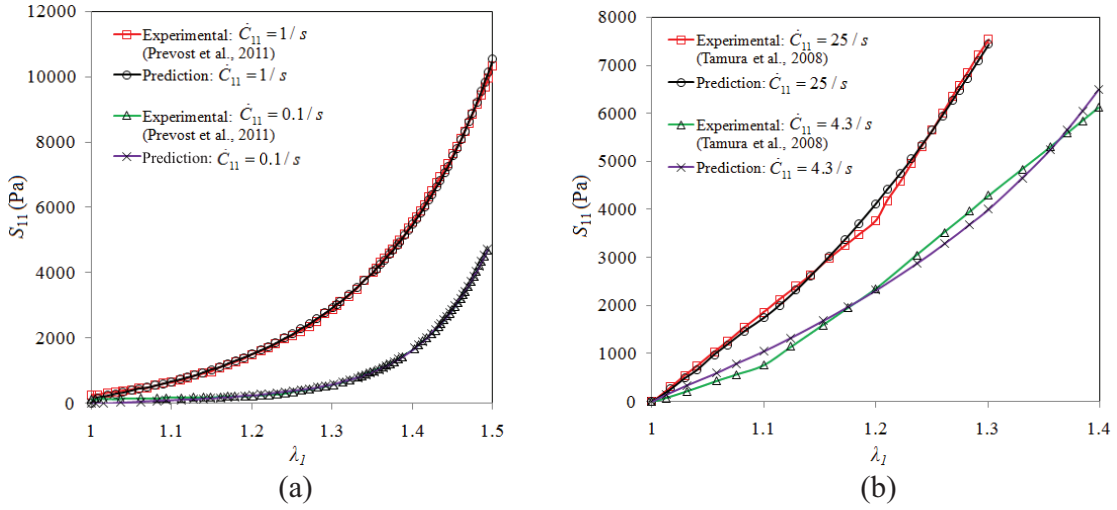

Figure 11. S_{11} (= $S_{11e} + S_{11v}$) vs. λ_1 for porcine brain tissues under uniaxial tensile loading at different strain rates.

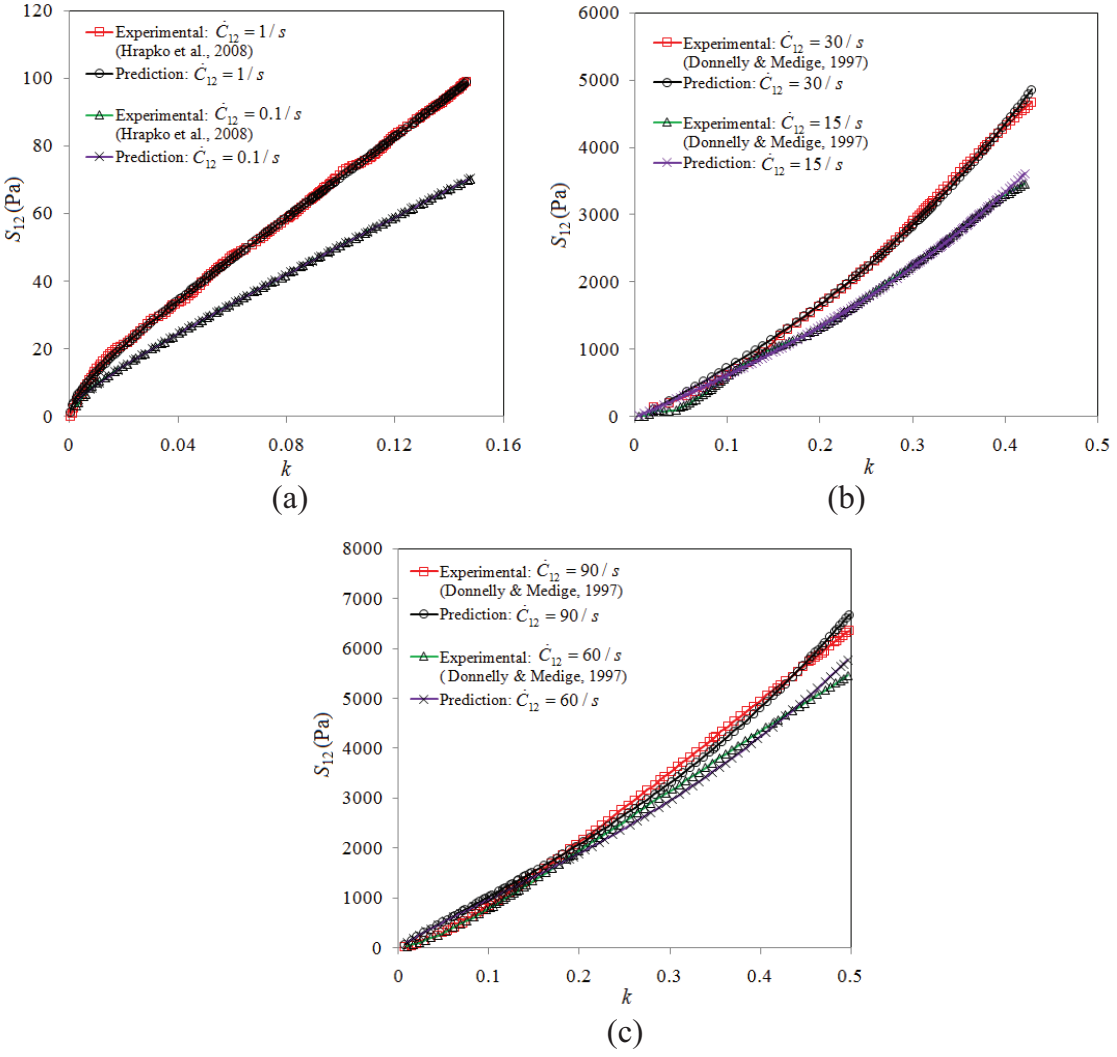

Figure 12. S_{12} (= $S_{12e} + S_{12v}$) vs. k under simple shear loading at different strain rates. The experimental data plotted in (a) are for porcine brain tissues, and those plotted in (b) and (c) are for human brain tissues.

Table 1. The rate-dependent viscous stress $\mathbf{S}_v$ computed using equation (57) is added to the quasi-static stress $\mathbf{S}_e = 2\dfrac{\partial W_e}{\partial \mathbf{C}} - p\mathbf{C}^{-1}$ (see equation (12(a))) to obtain the total stress $\mathbf{S} = \mathbf{S}_e + \mathbf{S}_v$ in the material. The parameters involved in equation (57) and used for computing $\mathbf{S}_v$ are listed in Tables 2 and 3.

Figure 11 shows the material response to uniaxial tensile loading at strain rates ranging from 0.1 /s to 25 /s. Figure 12 displays the response to simple shear loading at strain rates between 0.1 /s and 90 /s. The error in data fitting and success of minimization as indicated by the first-order optimality measure are displayed in Table 2 (for tensile loading) and Table 3 (for shear loading).

Clearly, Figures 11 and 12 show that the normal and shear stresses predicted by the current visco-hyperelastic model agree well with the experimental data available for the uniaxial loading [27, 22] and simple shear loading [24, 25] cases, even though a unique set of fitting parameters could not be found and used in fitting the experimental curves obtained at different strain rates shown in Figures 11 and 12. This non-uniqueness has been mathematically shown to occur for many models [61]. A unique set of fitting parameters can be estimated only if the identifiability criterion is satisfied, which requires that the sensitivity coefficients of the model be linearly independent over the range of the measurements. This criterion has been applied by De Vita and Slaughter [62] to show why their constitutive model for strain rate-dependent behavior of soft tissues (anterior cruciate ligaments) fits the experimental stress–strain curve of Pioletti et al. [63] at each strain rate very well but they could not determine a unique set of fitting parameters that can be used to accurately fit the experimental curves at various strain rates. By following the procedure discussed in Beck and Arnold [61] and used in De Vita and Slaughter [62], it can be readily shown that the identifiability criterion is not satisfied by the current rate-dependent model over the range of the measurements reported in Donnelly and Medige [25], Tamura et al. [27], Hrapko et al. [24], and Prevost et al. [22], thereby explaining the non-uniqueness of the fitting parameters. This limitation of the current model is similar to that exhibited by the constitutive model proposed in De Vita and Slaughter [62] and the well-known constitutive models of Fung, Mooney-Rivlin, Gent, and Ogden applied in Rashid et al. [28, 64, 65] for strain rate-dependent behavior of soft tissues.

5. Summary

A transversely isotropic visco-hyperelastic constitutive model is provided for soft tissues based on continuum mechanics. A new form of the strain energy density function based on five invariants of the right Cauchy-Green deformation tensor $\mathbf{C}$ is proposed to model quasi-static responses, and a rate-dependent viscous potential involving two invariants of $\dot{\mathbf{C}}$ (the total material time derivative of $\mathbf{C}$) additionally is suggested to account for short-term memory effects. The predicted stress responses by the newly proposed constitutive model compare well with available experimental data for porcine and human brain tissues and bovine pericardium at different strain rates and under multiple loading conditions. The model can be applied to other soft tissues by using different values of material and fitting parameters.

Acknowledgements

The authors wish to thank Professor David Steigmann and two anonymous reviewers for their encouragement and helpful comments on an earlier version of the paper.

Funding

The work reported here is partially funded by a contract from the US Army. This support is gratefully acknowledged. The views and conclusions contained herein are those of the authors and should not be interpreted as necessarily representing the official policies or endorsements, either expressed or implied, of the US Army.

References

[1] Humphrey, JD. Review paper: continuum biomechanics of soft biological tissues. *Proceedings Royal Soc A* 2003; 459: 3–46.

[2] Holzapfel, GA, and Ogden, RW. Constitutive modelling of arteries. *Proceedings Royal Soc A* 2010; 466: 1551–1597.

[3] Prange, MT, and Margulies, SS. Regional, directional, and age-depedent properties of the brain undergoing large deformation. *J Biomech Engr* 2002; 124(2): 244–252.
[4] Velardi, F, Fraternali, F, and Angelillo, M. Anisotropic constitutive equations and experimental tensile behavior of brain tissue. *Biomech Mod Mechanobio* 2006; 5(1): 53–61.
[5] Ning, X, Zhu, Q, Lanir, Y, et al. A transversely isotropic viscoelastic constitutive equation for brainstem undergoing finite deformation. *J Biomech Engr* 2006; 128(6): 925–933.
[6] Pervin, F, and Chen, WW. Dynamic mechanical response of bovine gray matter and white matter brain tissues under compression. *J Biomech* 2009; 42: 731–735.
[7] Sacks, MS, and Sun, W. Multiaxial mechanical behavior of biological materials. *Annual Rev Biomed Engr* 2003; 5: 251–284.
[8] Peng, XQ, Guo, ZY, and Moran, B. An anisotropic hyperelastic constitutive model with fiber-matrix shear interaction for the human annulus fibrosus. *ASME J Applied Mech* 2006; 73(5): 815–824.
[9] Zhurov, AI, Limbert, G, Aeschlimann, DP, et al. A constitutive model for the periodontal ligament as a compressible transversely isotropic visco-hyperelastic tissue. *Comp Meth Biomech Biomed Engr* 2007; 10(3): 223–235.
[10] Dokos, S, Smaill, BH, Young, AA, et al. Shear properties of passive ventricular myocardium. *Amer J Physio, Heart Circ Physio* 2002; 283: H2650–H2659.
[11] Holzapfel, GA, and Ogden, RW. Constitutive modeling of passive myocardium: a structurally based framework for material characterization. *Philos Trans Royal Soc London, Series A* 2009; 367: 3445–3475.
[12] Vaishnav, RN, Young, JT, Janicki, JS, et al. Nonlinear anisotropic elastic properties of the canine aorta. *Biophysics J* 1972; 12(8): 1008–1027.
[13] Fung, YC, Fronek, K, and Patitucci, P. Pseudoelasticity of arteries and choice of its mathematical expression. *Amer J Physio* 1979; 237: H620–H631.
[14] Holzapfel, GA, Gasser, TC, and Ogden, RW. A new constitutive framework for arterial wall mechanics and a comparative study of material models. *J Elasticity* 2000; 61: 1–48.
[15] Ciarletta, P, Izzo, I, Micera, S., et al. Stiffening by fiber reinforcement in soft materials: a hyperelastic theory at large strains and its application. *J Mech Behavior Biomed Mats* 2011; 4: 1359–1368.
[16] Horgan, CO, and Saccomandi, G. A new constitutive theory for fiber-reinforced incompressible nonlinearly elastic solids. *J Mech Physics Solids* 2005; 53: 1985–2015.
[17] Wu, HC, and Yao, RF. Mechanical behavior of human annulus fibrosis. *J Biomech* 1976; 9(1): 1–7.
[18] Criscione, JC, Douglas, AS, and Hunter, WC. Physically based strain invariant set for materials exhibiting transversely isotropic behavior. *J Mech Physics Solids* 2001; 49: 871–897.
[19] Lu, YT, Zhu, HX, Richmond, S, et al. Numerical modelling of the fibre-matrix interaction in biaxial loading for hyperelastic soft tissue models. *Internat J Numerical Methods Biomed Engr* 2012; 28: 401–411.
[20] Guo, ZY, Peng, XQ, and Moran, B. A composites-based hyperelastic constitutive model for soft tissue with application to the human annulus fibrosus. *J Mech Physics Solids* 2006; 54: 1952–1971.
[21] Guo, ZY, Peng, XQ, and Moran, B. Large deformation response of a hyperelastic fibre reinforced composite: theoretical model and numerical validation. *Composites Part A Applied Sci Manufact* 2007; 38: 1842–1851.
[22] Prevost, TP, Balakrishnan, A, Suresh, S., et al. Biomechanics of brain tissue. *Acta Biomat* 2011; 7(1): 83–95.
[23] Shuck, LZ, and Advani, SH. Rheological response of human brain tissue in shear. *ASME J Basic Engr* 1972; 94: 905–911.
[24] Hrapko, M, van Dommelen, JAW, Peters, GWM, et al. Characterisation of the mechanical behaviour of brain tissue in compression and shear. *Biorheology* 2008; 45: 663–676.
[25] Donnelly, BR, and Medige, J. Shear properties of human brain tissue. *J Biomech Engr* 1997; 119: 423–432.
[26] Tamura, A, Hayashi, S, Watanabe, I, et al. Mechanical characterization of brain tissue in high-rate compression. *J Biomech Sci Engr* 2007; 2(3): 115–126.
[27] Tamura, A, Hayashi, S, Nagayama, K, et al. Mechanical characterization of brain tissue in high-rate extension. *J Biomech Sci Engr* 2008; 3(2): 263–274.
[28] Rashid, B, Destrade, M, and Gilchrist, M. Mechanical characterization of brain tissue in compression at dynamic strain rates. *J Mech Behavior Biomed Mats* 2012; 10: 23–38.
[29] Kulkarni, S, Gao, X-L, Horner, SE, et al. (2013). Review: ballistic helmets — their design, materials, and performance against traumatic brain injury. *Comp Struct* 2013; 101: 313–331.
[30] Spencer, AJM. Theory of invariants. In: *Continuum physics, vol I*. New York: Academic Press, 1971.
[31] Boehler, JP. *Application of tensor functions in solid mechanics*. Vienna, Austria: Springer-Verlag, 1987.
[32] Zheng, Q-S. Theory of representations for tensor functions — a unified invariant approach to constitutive equations. *Applied Mech Rev* 1994; 47(11): 545–587.
[33] Spencer, AJM. *Deformations of fibre-reinforced materials*. Oxford: Clarendon Press, 1972.
[34] Ding, H-J, Chen, WQ, and Zhang, L. *Elasticity of transversely isotropic materials*, Dordrecht, The Netherlands: Springer, 2006.
[35] Gao, X-L, and Mao, CL. Solution of the contact problem of a rigid conical frustum indenting a transversely isotropic elastic half-space. *ASME J Applied Mech* 2014; 81: 041007-1–041007-12.

[36] Schröder, J, and Neff, P. Invariant formulation of hyperelastic transverse isotropy based on polyconvex free energy functions. *Internat J Solids Struct* 2003; 40: 401–445.
[37] Lu, J, and Zhang, L. Physically motivated invariant formulation for transversely isotropic hyperelasticity. *Internat J Solids Struct* 2005; 42: 6015–6031.
[38] Shariff, MHBM. Nonlinear transversely isotropic elastic solids: an alternative representation. *Quarterly J Mech Applied Maths* 2008; 61(2): 129–149.
[39] Pioletti, DP, and Rakotomanana, LR. Non-linear viscoelastic laws for soft biological tissues. *Euro J Mech Solids* 2000; 19(5): 749–759.
[40] Truesdell, C, Noll, W, and Antman, SS. *The non-linear field theories of mechanics*. Berlin, Germany: Springer-Verlag, 2004.
[41] Chatelin, S, Deck, C, and Willinger, R. An anisotropic viscous hyperelastic constitutive law for brain material finite-element modeling. *J Biorheology* 2013; 27: 26–37.
[42] Wright, RM, and Ramesh, KT. An axonal strain injury criterion for traumatic brain injury. *Biomech Mod Mechanobio* 2012; 11(1–2): 245–260.
[43] Dorfmann, AL, Woods, WAJr, and Trimmer, BA. Muscle performance in a soft-bodied terrestrial crawler: constitutive modelling of strain-rate depedency. *J Royal Soc, Interface* 2007; 5: 349–362.
[44] Merodio, J, and Ogden, RW. Material instabilities in fiber-reinforced nonlinearly elastic solids under plane deformation. *Acta Mechanica* 2002; 54(5–6): 525–552.
[45] Merodio, J, and Ogden, RW. Instabilities and loss of ellipticity in fiber-reinforced compressible non-linearly elastic solids under plane deformation. *Internat J Solids Struct* 2003; 40(18): 4707–4727.
[46] Merodio, J, and Ogden, RW. Mechanical response of fiber-reinforced incompressible non-linearly elastic solids. *Internat J Non-linear Mech* 2005; 40(2–3): 213–227.
[47] Balzani, D, Neff, P, Schröder, J, et al. A polyconvex framework for soft biological tissues. Adjustment to experimental data. *Internat J Solids Struct* 2006; 43: 6052–6070.
[48] Steigmann, DJ. Frame-invariant polyconvex strain energy functions for some anisotropic solids. *Maths Mech Solids* 2003; 8(5): 497–506.
[49] Schröder, J. *Poly-, quasi- and rank-one convexity in applied mechanics*. Berlin, Germany: Springer-Verlag, 2010.
[50] Destrade, M, Gilchrist, MD, Prikazchikov, DA, et al. Surface instability of sheared soft tissues. *J Biomech Engr* 2008; 130: 061007-1–061007-6.
[51] Holzapfel, GA. *Nonlinear solid mechanics: a continuum approach for engineering*. West Sussex, England: John Wiley & Sons Ltd, 2000.
[52] Sacks, MS. A method for planar biaxial mechanical testing that includes in-plane shear. *J Biomech Engr* 1999; 121(5): 551–555.
[53] Bass, EC, Ashford, FA, Segal, MR, et al. Biaxial testing of human annulus fibrosus and its implications for a constitutive formulation. *Annals Biomed Engr* 2004; 32: 1231–1242.
[54] Qiu, GY, and Pence, TJ. Remarks on the behavior of simple directionally reinforced incompressible nonlinearly elastic solids. *J Elasticity* 1997; 49(1): 1–30.
[55] Dokos, S, LeGrice, IJ, Smaill, BH, et al. A triaxial measurement shear-test device for soft biological tissues. *J Biomech Engr* 2000; 122: 471–478.
[56] Lee, EH. Elastic-plastic deformation at finite strains. *ASME J Applied Mech* 1969; 38: 1–6.
[57] Green, AE, and Naghdi, PM. Some remarks on elastic-pastic deformation at finite strain. *Internat J Engr Sci* 1971; 9: 1219–1229.
[58] Coleman, BD, and Noll, W. The thermodynamics of elastic materials with heat conduction and viscosity. *Archive Rational Mech Analysis* 1963; 13: 167–178.
[59] Limbert, G, and Middleton, J. A transversely isotropic viscohyperelastic material. Application to the modeling of biological soft connective tissues. *Internat J Solids Struct* 2004; 41: 4237–4260.
[60] Gurtin, ME, Fried, E, and Anand, L. *The mechanics and thermodynamics of continua*. New York: Cambridge University Press, 2010.
[61] Beck, JV, and Arnold, K J. *Parameter estimation in engineering and science*. New York: Wiley, 1977.
[62] De Vita, R, and Slaughter, WS. A structural constitutive model for the strain rate-dependent behavior of anterior cruciate ligaments. *Internat J Solids Struct* 2006; 43: 1561–1570.
[63] Pioletti, DP, Rakotomanana, LR, and Leyvraz, PK. Strain rate effect on the mechanical behavior of the anterior cruciate ligament-bone complex. *Med Engr Physics* 1999; 21: 95–100.
[64] Rashid, B, Destrade, M, and Gilchrist, M. Mechanical characterization of brain tissue in simple shear at dynamic strain rates. *J Mech Behavior Biomed Mats* 2013; 28: 71–85.
[65] Rashid, B, Destrade, M, and Gilchrist, M. Mechanical characterization of brain tissue in tension at dynamic strain rates. *J Mech Behavior Biomed Mats* 2014; 33: 43–54.
[66] Weiss, JA, Maker, BN, and Govindjee, S. Finite elememt implementation of incompressible, transversely isotropic hyperelasticity. *Comp Meth Applied Mech Engr* 1996; 135: 107–128.

Appendix: elasticity and viscosity tensors

Elasticity tensors, which are also known as linearized tangent moduli, are essential for finite element implementation of constitutive models.

Note from equation (52) that the second P-K stress $\mathbf{S}$ is a function of $\mathbf{C}$ and $\dot{\mathbf{C}}$. One can then write [59]

$$\mathbf{S} = \mathbf{E}_e : \mathbf{C} + \mathbf{E}_v : \dot{\mathbf{C}}, \tag{A1}$$

where

$$\mathbf{E}_e \equiv 2\frac{\partial \mathbf{S}_e}{\partial \mathbf{C}}, \quad \mathbf{E}_v \equiv 2\frac{\partial \mathbf{S}_v}{\partial \dot{\mathbf{C}}} \tag{A2a, b}$$

are the fourth-order elasticity and viscosity tensors, respectively. Using equations (49) and (53) in equations (A2a, b) gives

$$\mathbf{E}_e = 4\frac{\partial W_e}{\partial \mathbf{C}\partial \mathbf{C}}, \quad \mathbf{E}_v = 4\frac{\partial W_v}{\partial \dot{\mathbf{C}}\,\partial \dot{\mathbf{C}}}. \tag{A3a, b}$$

For transversely isotropic materials, $W_e(\mathbf{C}) = W_e(I_1, I_2, I_3, I_4, I_5)$ [33]. Using equation (A3a) then gives the elasticity tensor as

$$\begin{aligned}
\mathbf{E}_e = {} & 4\left(\frac{\partial^2 W_e}{\partial I_1 \partial I_1} + 2I_1\frac{\partial^2 W_e}{\partial I_1 \partial I_2} + \frac{\partial W_e}{\partial I_2} + I_1^2\frac{\partial^2 W_e}{\partial I_2 \partial I_2}\right)\mathbf{I}\otimes\mathbf{I} - 4\left(\frac{\partial^2 W_e}{\partial I_1 \partial I_2} + I_1\frac{\partial^2 W_e}{\partial I_2 \partial I_2}\right)(\mathbf{I}\otimes\mathbf{C} + \mathbf{C}\otimes\mathbf{I}) \\
& + 4\frac{\partial^2 W_e}{\partial I_2 \partial I_2}(\mathbf{C}\otimes\mathbf{C}) - 4\frac{\partial W_e}{\partial I_2}\mathbf{I}_4 + 4\left(\frac{\partial^2 W_e}{\partial I_1 \partial I_4} + I_1\frac{\partial^2 W_e}{\partial I_2 \partial I_4}\right)[\mathbf{I}\otimes(\mathbf{a}_0\otimes\mathbf{a}_0) + (\mathbf{a}_0\otimes\mathbf{a}_0)\otimes\mathbf{I}] \\
& - 4\frac{\partial^2 W_e}{\partial I_2 \partial I_4}[\mathbf{C}\otimes(\mathbf{a}_0\otimes\mathbf{a}_0) + (\mathbf{a}_0\otimes\mathbf{a}_0)\otimes\mathbf{C}] + 4\frac{\partial^2 W_e}{\partial I_4 \partial I_4}(\mathbf{a}_0\otimes\mathbf{a}_0\otimes\mathbf{a}_0\otimes\mathbf{a}_0) \\
& + 4\left(\frac{\partial^2 W_e}{\partial I_1 \partial I_5} + I_1\frac{\partial^2 W_e}{\partial I_2 \partial I_5}\right)[\mathbf{I}\otimes(\mathbf{a}_0\otimes\mathbf{C}\mathbf{a}_0 + \mathbf{C}\mathbf{a}_0\otimes\mathbf{a}_0) + (\mathbf{a}_0\otimes\mathbf{C}\mathbf{a}_0 + \mathbf{C}\mathbf{a}_0\otimes\mathbf{a}_0)\otimes\mathbf{I}] \\
& - 4\frac{\partial^2 W_e}{\partial I_2 \partial I_5}[\mathbf{C}\otimes(\mathbf{a}_0\otimes\mathbf{C}\mathbf{a}_0 + \mathbf{C}\mathbf{a}_0\otimes\mathbf{a}_0) + (\mathbf{a}_0\otimes\mathbf{C}\mathbf{a}_0 + \mathbf{C}\mathbf{a}_0\otimes\mathbf{a}_0)\otimes\mathbf{C}] \\
& + 4\frac{\partial^2 W_e}{\partial I_5 \partial I_5}[(\mathbf{a}_0\otimes\mathbf{C}\mathbf{a}_0 + \mathbf{C}\mathbf{a}_0\otimes\mathbf{a}_0)\otimes(\mathbf{a}_0\otimes\mathbf{C}\mathbf{a}_0 + \mathbf{C}\mathbf{a}_0\otimes\mathbf{a}_0)] \\
& + 4\frac{\partial^2 W_e}{\partial I_4 \partial I_5}[(\mathbf{a}_0\otimes\mathbf{a}_0)\otimes(\mathbf{a}_0\otimes\mathbf{C}\mathbf{a}_0 + \mathbf{C}\mathbf{a}_0\otimes\mathbf{a}_0) + (\mathbf{a}_0\otimes\mathbf{C}\mathbf{a}_0 + \mathbf{C}\mathbf{a}_0\otimes\mathbf{a}_0)\otimes(\mathbf{a}_0\otimes\mathbf{a}_0)] \\
& + 4\frac{\partial W_e}{\partial I_5}\frac{\partial^2 I_5}{\partial \mathbf{C}\partial \mathbf{C}} + 4\left(I_3\frac{\partial^2 W_e}{\partial I_1 \partial I_3} + I_1 I_3\frac{\partial^2 W_e}{\partial I_2 \partial I_3}\right)(\mathbf{I}\otimes\mathbf{C}^{-1} + \mathbf{C}^{-1}\otimes\mathbf{I}) \\
& - 4I_3\frac{\partial^2 W_e}{\partial I_2 \partial I_3}(\mathbf{C}\otimes\mathbf{C}^{-1} + \mathbf{C}^{-1}\otimes\mathbf{C}) + 4\left(I_3\frac{\partial W_e}{\partial I_3} + I_3^2\frac{\partial^2 W_e}{\partial I_3 \partial I_3}\right)(\mathbf{C}^{-1}\otimes\mathbf{C}^{-1}) \\
& + 4I_3\frac{\partial^2 W_e}{\partial I_3 \partial I_4}\left[(\mathbf{a}_0\otimes\mathbf{a}_0)\otimes\mathbf{C}^{-1} + \mathbf{C}^{-1}\otimes(\mathbf{a}_0\otimes\mathbf{a}_0)\right] \\
& + 4I_3\frac{\partial^2 W_e}{\partial I_3 \partial I_5}\left[(\mathbf{a}_0\otimes\mathbf{C}\mathbf{a}_0 + \mathbf{C}\mathbf{a}_0\otimes\mathbf{a}_0)\otimes\mathbf{C}^{-1} + \mathbf{C}^{-1}\otimes(\mathbf{a}_0\otimes\mathbf{C}\mathbf{a}_0 + \mathbf{C}\mathbf{a}_0\otimes\mathbf{a}_0)\right] + 4I_3\frac{\partial W_e}{\partial I_3}\frac{\partial \mathbf{C}^{-1}}{\partial \mathbf{C}},
\end{aligned} \tag{A4}$$

where $\mathbf{I}_4$ is the fourth-order identity tensor and use has been made of equation (15). For incompressible materials, the dependence of W_e on I_3 is suppressed, and equation (A4) reduces to that provided in Weiss et al. [66] (without the last 10 tensorial terms).

For transversely isotropic materials, $W_v(\dot{\mathbf{C}}) = W_v(J_1, J_2, J_3, J_4, J_5, J_6, J_7, J_8, J_9, J_{10}, J_{11}, J_{12})$ [31, 59], where J_2 and J_5 are defined in equation (56), and the other 10 invariants are given by

$$\begin{aligned} &J_1 = tr\left(\dot{\mathbf{C}}\right), \quad J_3 = \det\left(\dot{\mathbf{C}}\right), \quad J_4 = (\mathbf{a}_0 \otimes \mathbf{a}_0) : \dot{\mathbf{C}}, \quad J_6 = tr\left(\mathbf{C}\,\dot{\mathbf{C}}\right), \quad J_7 = tr\left(\mathbf{C}\,\dot{\mathbf{C}}^2\right), \quad J_8 = tr\left(\mathbf{C}^2\,\dot{\mathbf{C}}\right), \\ &J_9 = tr\left(\mathbf{C}^2\,\dot{\mathbf{C}}^2\right), \quad J_{10} = tr\left[(\mathbf{a}_0 \otimes \mathbf{a}_0)\mathbf{C}\,\dot{\mathbf{C}}\right], \quad J_{11} = tr\left[(\mathbf{a}_0 \otimes \mathbf{a}_0)\mathbf{C}\,\dot{\mathbf{C}}^2\right], \quad J_{12} = tr\left[(\mathbf{a}_0 \otimes \mathbf{a}_0)\mathbf{C}^2\,\dot{\mathbf{C}}\right]. \end{aligned} \tag{A5}$$

It then follows from equations (53), (56), and (A5) that

$$\begin{aligned} \mathbf{S}_v = {} & 2\frac{\partial W_v}{\partial J_1}\mathbf{I} + 2\frac{\partial W_v}{\partial J_2}\dot{\mathbf{C}} + 2J_3\frac{\partial W_v}{\partial J_3}\dot{\mathbf{C}}^{-1} + 2\frac{\partial W_v}{\partial J_4}\mathbf{a}_0 \otimes \mathbf{a}_0 + 2\frac{\partial W_v}{\partial J_5}\left(\mathbf{a}_0 \otimes \dot{\mathbf{C}}\,\mathbf{a}_0 + \dot{\mathbf{C}}\,\mathbf{a}_0 \otimes \mathbf{a}_0\right) \\ & + 2\frac{\partial W_v}{\partial J_6}\mathbf{C} + 2\frac{\partial W_v}{\partial J_7}\left(\mathbf{C}\,\dot{\mathbf{C}} + \dot{\mathbf{C}}\,\mathbf{C}\right) + 2\frac{\partial W_v}{\partial J_8}\mathbf{C}^2 + 2\frac{\partial W_v}{\partial J_9}\left(\mathbf{C}^2\,\dot{\mathbf{C}} + \dot{\mathbf{C}}\,\mathbf{C}^2\right) + 2\frac{\partial W_v}{\partial J_{10}}\mathbf{C}(\mathbf{a}_0 \otimes \mathbf{a}_0) \\ & + 2\frac{\partial W_v}{\partial J_{11}}\left[\mathbf{C}\mathbf{a}_0 \otimes \dot{\mathbf{C}}\,\mathbf{a}_0 + \dot{\mathbf{C}}\,\mathbf{C}(\mathbf{a}_0 \otimes \mathbf{a}_0)\right] + 2\frac{\partial W_v}{\partial J_{12}}\mathbf{C}^2(\mathbf{a}_0 \otimes \mathbf{a}_0), \end{aligned} \tag{A6}$$

where use has been made of the following results:

$$\begin{aligned} &\frac{\partial J_1}{\partial \dot{\mathbf{C}}} = \mathbf{I}, \quad \frac{\partial J_2}{\partial \dot{\mathbf{C}}} = \dot{\mathbf{C}}, \quad \frac{\partial J_3}{\partial \dot{\mathbf{C}}} = J_3\,\dot{\mathbf{C}}^{-1}, \quad \frac{\partial J_4}{\partial \dot{\mathbf{C}}} = \mathbf{a}_0 \otimes \mathbf{a}_0, \quad \frac{\partial J_5}{\partial \dot{\mathbf{C}}} = \mathbf{a}_0 \otimes \dot{\mathbf{C}}\mathbf{a}_0 + \dot{\mathbf{C}}\mathbf{a}_0 \otimes \mathbf{a}_0, \quad \frac{\partial J_6}{\partial \dot{\mathbf{C}}} = \mathbf{C}, \\ &\frac{\partial J_7}{\partial \dot{\mathbf{C}}} = \mathbf{C}\,\dot{\mathbf{C}} + \dot{\mathbf{C}}\,\mathbf{C}, \quad \frac{\partial J_8}{\partial \dot{\mathbf{C}}} = \mathbf{C}^2, \quad \frac{\partial J_9}{\partial \dot{\mathbf{C}}} = \mathbf{C}^2\,\dot{\mathbf{C}} + \dot{\mathbf{C}}\,\mathbf{C}^2, \quad \frac{\partial J_{10}}{\partial \dot{\mathbf{C}}} = \mathbf{C}(\mathbf{a}_0 \otimes \mathbf{a}_0), \\ &\frac{\partial J_{11}}{\partial \dot{\mathbf{C}}} = \mathbf{C}\mathbf{a}_0 \otimes \dot{\mathbf{C}}\,\mathbf{a}_0 + \dot{\mathbf{C}}\,\mathbf{C}(\mathbf{a}_0 \otimes \mathbf{a}_0), \quad \frac{\partial J_{12}}{\partial \dot{\mathbf{C}}} = \mathbf{C}^2(\mathbf{a}_0 \otimes \mathbf{a}_0). \end{aligned} \tag{A7}$$

Substituting equation (A6) into equation (A2b) will lead to the general expression of the viscosity tensor involving all 12 invariants J_1–J_{12}. This expression would be very long. A compact form for the viscosity tensor was provided in Limbert and Middleton [59] using a different notation.

When only the first five invariants of $\dot{\mathbf{C}}$ are considered in the viscous potential W_v, i.e., $W_v = W_v(J_1, J_2, J_3, J_4, J_5)$, which includes the viscous potential proposed in the current study (see equation (55)) as a special case, the viscosity tensor can be explicitly obtained from equations (A3b), (56), (A5) and (A7) as

$$\begin{aligned} \mathbf{E}_v = {} & 4\frac{\partial^2 W_v}{\partial J_1 \partial J_1}\mathbf{I} \otimes \mathbf{I} + 4\frac{\partial^2 W_v}{\partial J_1 \partial J_2}(\mathbf{I} \otimes \dot{\mathbf{C}} + \dot{\mathbf{C}} \otimes \mathbf{I}) + 4J_3\frac{\partial^2 W_v}{\partial J_1 \partial J_3}(\mathbf{I} \otimes \dot{\mathbf{C}}^{-1} + \dot{\mathbf{C}}^{-1} \otimes \mathbf{I}) \\ & + 4\frac{\partial^2 W_v}{\partial J_1 \partial J_4}[\mathbf{I} \otimes (\mathbf{a}_0 \otimes \mathbf{a}_0) + (\mathbf{a}_0 \otimes \mathbf{a}_0) \otimes \mathbf{I}] \\ & + 4\frac{\partial^2 W_v}{\partial J_1 \partial J_5}\left[\mathbf{I} \otimes (\mathbf{a}_0 \otimes \dot{\mathbf{C}}\,\mathbf{a}_0 + \dot{\mathbf{C}}\,\mathbf{a}_0 \otimes \mathbf{a}_0) + (\mathbf{a}_0 \otimes \dot{\mathbf{C}}\,\mathbf{a}_0 + \dot{\mathbf{C}}\,\mathbf{a}_0 \otimes \mathbf{a}_0) \otimes \mathbf{I}\right] \\ & + 4\frac{\partial^2 W_v}{\partial J_2 \partial J_2}(\dot{\mathbf{C}} \otimes \dot{\mathbf{C}}) + 4J_3\frac{\partial^2 W_v}{\partial J_2 \partial J_3}(\dot{\mathbf{C}} \otimes \dot{\mathbf{C}}^{-1} + \dot{\mathbf{C}}^{-1} \otimes \dot{\mathbf{C}}) \\ & + 4\frac{\partial^2 W_v}{\partial J_2 \partial J_4}[\dot{\mathbf{C}} \otimes (\mathbf{a}_0 \otimes \mathbf{a}_0) + (\mathbf{a}_0 \otimes \mathbf{a}_0) \otimes \dot{\mathbf{C}}] \end{aligned}$$

$$
\begin{aligned}
&+4\frac{\partial^2 W_v}{\partial J_2 \partial J_5}[\dot{\mathbf{C}}\otimes(\mathbf{a}_0\otimes\dot{\mathbf{C}}\,\mathbf{a}_0+\dot{\mathbf{C}}\,\mathbf{a}_0\otimes\mathbf{a}_0)+(\mathbf{a}_0\otimes\dot{\mathbf{C}}\,\mathbf{a}_0+\dot{\mathbf{C}}\,\mathbf{a}_0\otimes\mathbf{a}_0)\otimes\dot{\mathbf{C}}]\\
&+4\frac{\partial W_v}{\partial J_2}\mathbf{I}_4+4J_3\left(\frac{\partial W_v}{\partial J_3}+J_3\frac{\partial^2 W_v}{\partial J_3\partial J_3}\right)\dot{\mathbf{C}}^{-1}\otimes\dot{\mathbf{C}}^{-1}+4J_3\frac{\partial^2 W_v}{\partial J_3\partial J_4}[(\mathbf{a}_0\otimes\mathbf{a}_0)\otimes\dot{\mathbf{C}}^{-1}+\dot{\mathbf{C}}^{-1}\otimes(\mathbf{a}_0\otimes\mathbf{a}_0)]\\
&+4J_3\frac{\partial^2 W_v}{\partial J_3\partial J_5}[(\mathbf{a}_0\otimes\dot{\mathbf{C}}\,\mathbf{a}_0+\dot{\mathbf{C}}\,\mathbf{a}_0\otimes\mathbf{a}_0)\otimes\dot{\mathbf{C}}^{-1}+\dot{\mathbf{C}}^{-1}\otimes(\mathbf{a}_0\otimes\dot{\mathbf{C}}\,\mathbf{a}_0+\dot{\mathbf{C}}\,\mathbf{a}_0\otimes\mathbf{a}_0)]\\
&+4J_3\frac{\partial W_v}{\partial J_3}\frac{\partial\dot{\mathbf{C}}^{-1}}{\partial\dot{\mathbf{C}}}+4\frac{\partial^2 W_v}{\partial J_4\partial J_4}(\mathbf{a}_0\otimes\mathbf{a}_0\otimes\mathbf{a}_0\otimes\mathbf{a}_0)\\
&+4\frac{\partial^2 W_v}{\partial J_4\partial J_5}[(\mathbf{a}_0\otimes\mathbf{a}_0)\otimes(\mathbf{a}_0\otimes\dot{\mathbf{C}}\,\mathbf{a}_0+\dot{\mathbf{C}}\,\mathbf{a}_0\otimes\mathbf{a}_0)+(\mathbf{a}_0\otimes\dot{\mathbf{C}}\,\mathbf{a}_0+\dot{\mathbf{C}}\,\mathbf{a}_0\otimes\mathbf{a}_0)\otimes(\mathbf{a}_0\otimes\mathbf{a}_0)]\\
&+4\frac{\partial^2 W_v}{\partial J_5\partial J_5}(\mathbf{a}_0\otimes\dot{\mathbf{C}}\,\mathbf{a}_0+\dot{\mathbf{C}}\,\mathbf{a}_0\otimes\mathbf{a}_0)\otimes(\mathbf{a}_0\otimes\dot{\mathbf{C}}\,\mathbf{a}_0+\dot{\mathbf{C}}\,\mathbf{a}_0\otimes\mathbf{a}_0)+4\frac{\partial W_v}{\partial J_5}\frac{\partial^2 J_5}{\partial\dot{\mathbf{C}}\,\partial\dot{\mathbf{C}}}.
\end{aligned}
\tag{A8}
$$

Note that equations (A4) and (A8) are in the material description. The elasticity tensor $\mathbf{E}_e$ and viscosity tensor $\mathbf{E}_v$ in the spatial description can be respectively obtained from the Piola transformation of the corresponding tensor in the material description [51].

For the strain energy density function W_e (see equation (22)) and the viscous potential function W_v (see equation (55)) proposed in the current study, the elasticity tensor $\mathbf{E}_e$ and the viscosity tensor $\mathbf{E}_v$ can be obtained by directly using equations (A4) and (A8).